Experimental aspects of SU(5)×U(1) supergravity

Jorge L. Lopez,[1,2] D. V. Nanopoulos,[1-3] Gye T. Park,[1,2] Xu Wang,[1,2] and A. Zichichi[4]
[1]*Center for Theoretical Physics, Department of Physics, Texas A&M University, College Station, Texas 77843-4242*
[2]*Astroparticle Physics Group, Houston Advanced Research Center (HARC), The Mitchell Campus, The Woodlands, Texas 77381*
[3]*CERN, Theory Division, 1211 Geneva 23, Switzerland*
[4]*CERN, 1211 Geneva 23, Switzerland*
(Received 27 January 1994)

We study various aspects of SU(5)×U(1) supergravity as they relate to the experimental verification or falsification of this model. We consider two string-inspired, universal, one-parameter, no-scale soft-supersymmetry-breaking scenarios, driven by the F terms of the moduli and dilaton fields. The model is described in terms of the supersymmetry mass scale (i.e., the chargino mass $m_{\chi_1^\pm}$), $\tan\beta$, and the top-quark mass. We first determine the combined effect on the parameter space of all presently available direct and indirect experimental constraints, including the CERN LEP lower bounds on sparticle and Higgs-boson masses, the $b\to s\gamma$ rate, the anomalous magnetic moment of the muon, the high-precision electroweak parameters ϵ_1, ϵ_b (which imply $m_t \lesssim 180$ GeV), and the muon fluxes in underground detectors (neutrino telescopes). For the still-allowed points in $(m_{\chi_1^\pm}, \tan\beta)$ parameter space, we reevaluate the experimental situation at the Fermilab Tevatron, LEP II, and DESY HERA. In the 1994 run, the Tevatron could probe chargino masses as high as 100 GeV. At LEP II the parameter space could be explored with probes of different resolutions: Higgs-boson searches, selectron searches, and chargino searches. Moreover, for $m_t \lesssim 150$ GeV, these Higgs-boson searches could explore all of the allowed parameter space with $\sqrt{s} \lesssim 210$ GeV.

PACS number(s): 12.10.Dm, 04.65.+e, 14.80.Ly

I. INTRODUCTION

In the search for physics beyond the standard model, what is needed are detailed calculations to be confronted with experimental data. The starting point is the choice of a model described by the least numbers of parameters, and based on well-motivated theoretical assumptions. Our choice is SU(5)×U(1) supergravity [1], the reasons being twofold: first, because this model is derivable from string theory; second, because the SU(5)×U(1) gauge group is the simplest unified gauge extension of the standard model. It is unified because the two non-Abelian gauge couplings of the standard model (α_2 and α_3) are unified into the SU(5) gauge coupling. It is the simplest extension because this is the smallest unified group which provides neutrino masses. In this interpretation, minimal SU(5) would appear as a subgroup of SO(10), if it is to allow for neutrino masses. Moreover, the matter representations of SU(5)×U(1) entail several simplifications [2]. The most important are (i) the breaking of the gauge group via vacuum expectation values of $\mathbf{10}, \overline{\mathbf{10}}$ Higgs fields, (ii) the natural splitting of the doublet and triplet components of the Higgs pentaplets and therefore the natural avoidance of dangerous dimension-five proton decay operators, and (iii) the natural appearance of a seesaw mechanism for neutrino masses. In the context of string model building, the SU(5)×U(1) structure becomes even more important, since the traditional grand unified gauge groups [SU(5),SO(10),E_6] cannot be broken down to the standard model gauge group in the simplest (and to date almost unique) string constructions, because of the absence of adjoint Higgs representations [3]. This reasoning is not applicable to the SU(5)×U(1) gauge group, since the required $\mathbf{10}, \overline{\mathbf{10}}$ representations are very common in string model building [4–6].

We supplement the SU(5)×U(1) gauge group choice with the minimal matter content which allows it to unify at the string scale $M_U \sim 10^{18}$ GeV, as expected to occur in the string-derived versions of the model [7,8]. This entails a set of intermediate-scale mass particles: a vectorlike quark doublet with mass $m_Q \sim 10^{12}$ GeV and a vectorlike charge $-\frac{1}{3}$ quark singlet with mass $m_D \sim 10^6$ GeV [9,10]. The model is also implicitly constrained by the requirement of suitable supersymmetry breaking. We choose two string-inspired scenarios which have the virtue of yielding universal soft-supersymmetry-breaking parameters $(m_{1/2}, m_0, A)$, in contrast with nonuniversal soft-supersymmetry-breaking scenarios which occur quite commonly in string constructions [11–13] and may be phenomenologically troublesome [14]. These scenarios are examples of the no-scale supergravity framework [15,16] in which the dimensional parameters of the theory are undetermined at the classical level, but are fixed by radiative corrections, thus including the whole theory in the determination of the low-energy parameters. In the *moduli* scenario, supersymmetry breaking is driven by the vacuum expectation value (VEV) of the moduli fields (T), and gives $m_0 = A = 0$, while in the *dilaton* scenario [12,13] supersymmetry breaking is driven by the VEV of the dilaton field (S) and entails

$m_0=(1/\sqrt{3})m_{1/2}$, $A=-m_{1/2}$. Thus, the supersymmetry-breaking sector depends on only one parameter (i.e., $m_{1/2}$).

The parameter space of SU(5)×U(1) supergravity is fully described by just two more quantities: the ratio of Higgs-boson vacuum expectation values (tanβ), and the top-quark mass (m_t). This three-dimensional parameter space (i.e., $m_{1/2}$, tanβ, and m_t) has been explored in detail in Refs. [10,17] for the moduli and dilaton scenarios, respectively. The allowed points in parameter space are determined by a theoretical procedure (including renormalization-group evolution of the model parameters from the unification scale down to the electroweak scale and enforcement of radiative electroweak symmetry breaking using the one-loop effective potential) and by the further imposition of the basic constraints from the CERN e^+e^- collider LEP on the sparticle and Higgs-boson masses, as described in Ref. [18]. More recently, we have investigated further constraints on the parameter space, including (i) the CLEO limits on the $b\to s\gamma$ rates [19,20], (ii) the long-standing limit on the anomalous magnetic moment of the muon [21], (iii) the electroweak high-precision LEP measurements in the form of the ϵ_1,ϵ_b parameters [22,20,23] (here we update our analysis including the latest LEP data), (iv) the nonobservation of anomalous muon fluxes in underground detectors ("neutrino telescopes") [24], and (v) the possible constraints from trilepton searches at the Fermilab Tevatron [25].

In our analysis we combine the most useful elements of the top-down and bottom-up approaches to physics beyond the standard model. The top-down approach consists of selecting particularly well-motivated string-inspired scenarios for supersymmetry breaking (i.e., with a single mass parameter), whereas the bottom-up approach aims at imposing all known direct and indirect experimental constraints on the chosen model. In this way, we can corner the high-energy parameter space of the model (bottom-up) and thus focus our search for further realistic supersymmetric models (top-down). On the other hand, the completely phenomenological approach in which the many parameters (more than 20) of the minimal supersymmetric standard model (MSSM) are arbitrarily varied, is neither practical nor illuminating.

It is important to note that our advocacy of supersymmetry, as the choice for physics beyond the standard model, seems to be accumulating indirect supporting evidence: (i) global fits to the electroweak sector of the standard model show a preference for a light Higgs boson [26], in agreement with low-energy supersymmetry where a light Higgs boson is always present; (ii) the precisely measured gauge couplings, when extrapolated to very high energies using standard model radiative effects, fail to converge at any high-energy scale [27,28], consistent with the fate of nonsupersymmetric grand unified theories (GUT's) in light of the gauge hierarchy problem; (iii) on the contrary, in the supersymmetric version of the standard model, the gauge couplings unify at a scale $M_U\sim 10^{16}$ GeV [28]; (iv) global fits to the electroweak data also imply that $m_t=140\pm 20$ GeV for $m_H=60$ GeV and $m_t=180\pm 18$ GeV for $m_H=1$ TeV (see, e.g., Refs. [29,30]), consistent with the radiative electroweak symmetry breaking mechanism [31,16]; (v) $m_t\lesssim 190$–200 GeV (see, e.g., Ref. [32]) is required in a supersymmetric unified theory, consistent with the electroweak fits to m_t; and (vi) the resulting top-quark Yukawa couplings at the unification scale are naturally obtained in supersymmetric string models [4,5].

In this paper we first briefly review the basic SU(5)×U(1) supergravity properties (Sec. II), and then discuss each of the constraints on the parameter space separately (Sec. III), and also their combined effect (Sec. IV). Next we address the prospects for detecting the sparticles and Higgs bosons directly through searches at the Tevatron, LEP II, and the DESY *ep* collider HERA (Sec. V). We conclude that with the present generation of collider facilities, direct searches for the lighter weakly interacting sparticles and Higgs bosons probe the parameter space of SU(5)×U(1) supergravity in a much deeper way than direct searches for the heavier strongly interacting sparticles do. Moreover, within the weakly interacting sparticles, the deepest probe is provided by the lightest Higgs boson, followed by the selectrons, and then by the charginos. We also discuss the two most efficient ways of exploring the parameter space in the near future in an indirect way (Sec. VI), namely, through more precise $B(b\to s\gamma)$ and $(g-2)_\mu$ measurements. We summarize our conclusions in Sec. VII.

II. SU(5)×U(1) SUPERGRAVITY

A. Model building

The supergravity model of interest is based on the gauge group SU(5)×U(1) and is best motivated as a possible solution to string theory. In this regard several of its features become singularly unique, as discussed in the Introduction. However, string models (such as the one in Ref. [6]) are quite complicated and their phenomenology tends to be obscured by a number of new string parameters (although these could in principle be determined dynamically). It is therefore more convenient to study the phenomenology of a "string-inspired" model [10] which contains all the desirable features of the real string model, but where several simplifying assumptions have been made, as "inspired" by the detailed calculations in the real model. The string-inspired model is such that unification of the low-energy gauge couplings of the standard model occurs at the string scale $M_U\sim 10^{18}$ GeV. This is a simplifying assumption since in the string model there are several intermediate-scale particles which in effect produce a threshold structure as the string scale is approached. Perhaps because of this simplifying assumption, in the string-inspired model one seems to be forced to introduce nonminimal matter representations at intermediate scales: a vectorlike quark doublet with mass $m_Q\sim 10^{12}$ GeV and a vectorlike charge $-\frac{1}{3}$ quark singlet with mass $m_D\sim 10^6$ GeV [9,10]. The low-energy spectrum of the model contains the same sparticles and Higgs bosons as the minimal supersymmetric standard model (MSSM).

A very important component of the model is that which triggers supersymmetry breaking. In the string

model this task is performed by the hidden sector and the universal moduli and dilaton fields. Model-dependent calculations are required to determine the precise nature of supersymmetry breaking in a given string model. In fact, no explicit string model exists to date where various theoretical difficulties (e.g., suitably suppressed cosmological constant, suitable vacuum state with perturbative gauge coupling, etc.) have been satisfactorily overcome. Instead, it has become apparent [11–13] that a more model-independent approach to the problem may be more profitable. In this approach one parametrizes the breaking of supersymmetry by the largest F-term vacuum expectation value which triggers supersymmetry breaking. Of all the possible fields which could be involved (i.e., hidden sector matter fields, various moduli fields, dilaton) the dilaton and three of the moduli fields are quite common in string constructions and have thus received the most attention in the literature. In a way, if supersymmetry breaking is triggered by these fields (i.e., $\langle F_S\rangle\neq 0$ or $\langle F_T\rangle\neq 0$), this would be a rather generic prediction of string theory.

There are various possible scenarios for supersymmetry breaking that are obtained in this model-independent way. To discriminate among these we consider a simplified expression for the scalar masses (e.g., $m_{\tilde{q}}$) $\tilde{m}_i^2=m_{3/2}^2(1+n_i\cos^2\theta)$, with $\tan\theta=\langle F_S\rangle/\langle F_T\rangle$ [13]. Here $m_{3/2}$ is the gravitino mass and the n_i are the modular weights of the respective matter field. There are two ways in which one can obtain universal scalar masses, as desired phenomenologically to avoid large flavor-changing-neutral currents (FCNC's) [14]: (i) setting $\theta=\pi/2$, that is $\langle F_S\rangle\gg\langle F_T\rangle$; or (ii) in a model where all n_i are the same, as occurs for $Z_2\times Z_2$ orbifolds [13] and free-fermionic constructions [8].

In the first ("dilaton") scenario, supersymmetry breaking is triggered by the dilaton F term and yields universal soft-supersymmetry-breaking gaugino and scalar masses and trilinear interactions [12,13]:

$$m_0=\frac{1}{\sqrt{3}}m_{1/2},\quad A=-m_{1/2}\ . \tag{1}$$

In the second ("moduli") scenario, in the limit $\langle F_T\rangle\gg\langle F_S\rangle$ (i.e., $\theta\to 0$) all scalar masses at the unification scale vanish, as is the case in no-scale supergravity models with a unified group structure [16]. In this case we have

$$m_0=0,\quad A=0\ . \tag{2}$$

The procedure to extract the low-energy predictions of the model outlined above is rather standard (see, e.g., Ref. [18]): (a) the bottom-quark and τ-lepton masses, together with the input values of m_t and $\tan\beta$ are used to determine the respective Yukawa couplings at the electroweak scale; (b) the gauge and Yukawa couplings are then run up to the unification scale $M_U=10^{18}$ GeV taking into account the intermediate-scale particles introduced above; (c) at the unification scale the soft-supersymmetry-breaking parameters are introduced [according to Eqs. (1) and (2)] and the scalar masses are then run down to the electroweak scale; (d) radiative electroweak symmetry breaking is enforced by minimizing the one-loop effective potential which depends on the whole mass spectrum, and the values of the Higgs mixing term $|\mu|$ and the bilinear soft-supersymmetry-breaking parameter B are determined from the minimization conditions; (e) all known phenomenological constraints on the sparticle and Higgs-boson masses are applied (most importantly the LEP lower bounds on the chargino and Higgs masses), including the cosmological requirement of a not-too-large neutralino relic density (which happens to be satisfied automatically).

In either of the supersymmetry-breaking scenarios considered, after enforcement of the above constraints, the low-energy theory can be described in terms of just three parameters: the top-quark mass (m_t), the ratio of Higgs vacuum expectation values ($\tan\beta$), and the gaugino mass ($m_{1/2}$). Therefore, measurement of only two sparticle or Higgs-boson masses would determine the remaining thirty. Moreover, if the hidden sector responsible for these patterns of soft-supersymmetry-breaking is specified (as in a string-derived model), then the gravitino mass will also be determined and the supersymmetry breaking sector of the theory will be completely fixed.

B. Mass ranges

We have scanned the three-dimensional parameter space for $m_t=130,150,170$ GeV, $\tan\beta=2\to 50$, and $m_{1/2}=50\to 500$ GeV. Imposing the constraint $m_{\tilde{g}},m_{\tilde{q}}<1$ TeV we find

$$\text{moduli: } m_{1/2}<475\text{ GeV},\quad \tan\beta\lesssim 32\ , \tag{3}$$

$$\text{dilaton: } m_{1/2}<465\text{ GeV},\quad \tan\beta\lesssim 46\ . \tag{4}$$

These restrictions on $m_{1/2}$ cut off the growth of most of the sparticle and Higgs-boson masses at ≈ 1 TeV. However, the sleptons, the lightest Higgs boson, the two lightest neutralinos, and the lightest chargino are cut off at a much lower mass, as follows:[1]

$$\text{moduli: } \begin{cases} M_{\tilde{e}_R}<190\text{ GeV},\quad m_{\tilde{e}_L}<305\text{ GeV},\quad m_{\tilde{\nu}}<295\text{ GeV}, \\ m_{\tilde{\tau}_1}<185\text{ GeV},\quad m_{\tilde{\tau}_2}<315\text{ GeV}, \\ m_h<125\text{ GeV}, \\ m_{\chi_1^0}<145\text{ GeV},\quad m_{\chi_2^0}<290\text{ GeV},\quad m_{\chi_1^\pm}<290\text{ GeV}\ , \end{cases} \tag{5}$$

[1]In this class of supergravity models the three sneutrinos ($\tilde{\nu}$) are degenerate in mass. Also, $m_{\tilde{\mu}_L}=m_{\tilde{e}_L}$ and $m_{\tilde{\mu}_R}=m_{\tilde{e}_R}$.

$$\text{dilaton:}\quad \begin{cases} m_{\tilde{e}_R} < 325 \text{ GeV}, \quad m_{\tilde{e}_L} < 400 \text{ GeV}, \quad m_{\tilde{\nu}} < 400 \text{ GeV}, \\ m_{\tilde{\tau}_1} < 325 \text{ GeV}, \quad m_{\tilde{\tau}_2} < 400 \text{ GeV}, \\ m_h < 125 \text{ GeV}, \\ m_{\chi_1^0} < 145 \text{ GeV}, \quad m_{\chi_2^0} < 285 \text{ GeV}, \quad m_{\chi_1^\pm} < 285 \text{ GeV} . \end{cases} \tag{6}$$

It is interesting to note that because of the various constraints on the model, the gluino and (average) squark masses are bounded from below:

$$\begin{aligned} &\text{moduli:} \quad \begin{cases} m_{\tilde{g}} \gtrsim 245(260) \text{ GeV}, \\ m_{\tilde{q}} \gtrsim 240(250) \text{ GeV} , \end{cases} \\ &\text{dilaton:} \quad \begin{cases} m_{\tilde{g}} \gtrsim 195(235) \text{ GeV}, \\ m_{\tilde{q}} \lesssim 195(235) \text{ GeV} , \end{cases} \end{aligned} \tag{7}$$

for $\mu > 0 (\mu < 0)$. Relaxing the above conditions on $m_{1/2}$ simply allows all sparticle masses to grow further proportional to $m_{\tilde{g}}$.

C. Mass relations

The neutralino and chargino masses show a correlation observed before in this class of models [33,10]: namely (see Fig. 1, top row),

$$\begin{aligned} &m_{\chi_1^0} \approx \tfrac{1}{2} m_{\chi_2^0} , \\ &m_{\chi_2^0} \approx m_{\chi_1^\pm} \approx M_2 = (\alpha_2/\alpha_3) m_{\tilde{g}} \approx 0.28 m_{\tilde{g}} . \end{aligned} \tag{8}$$

This is because throughout the parameter space $|\mu|$ is generally much larger than M_W (see Fig. 1, bottom row) and $|\mu| > M_2$. In practice we find $m_{\chi_2^0} \approx m_{\chi_1^\pm}$ to be satisfied quite accurately, whereas $m_{\chi_1^0} \approx \frac{1}{2} m_{\chi_2^0}$ is only qualitatively satisfied, although the agreement is better in the dilaton case. In fact, these two mass relations are much more reliable than the one that links them to $m_{\tilde{g}}$. The heavier neutralino ($\chi_{3,4}^0$) and chargino ($\chi_2^\pm$) masses are determined by the value of $|\mu|$; they all approach this limit for large enough $|\mu|$. More precisely, $m_{\chi_3^0}$ approaches $|\mu|$ sooner than $m_{\chi_4^0}$ does. On the other hand, $m_{\chi_4^0}$ approaches $m_{\chi_2^\pm}$ rather quickly.

The first- and second-generation squark and slepton masses can be determined analytically:

$$\begin{aligned} \tilde{m}_i &= \left[m_{1/2}^2 (c_i + \xi_0^2) - d_i \frac{\tan^2\beta - 1}{\tan^2\beta + 1} M_W^2 \right]^{1/2} \\ &= a_i m_{\tilde{g}} \left[1 + b_i \left[\frac{150}{m_{\tilde{g}}} \right]^2 \frac{\tan^2\beta - 1}{\tan^2\beta + 1} \right]^{1/2} , \end{aligned} \tag{9}$$

where $d_i = (T_{3i} - Q)\tan^2\theta_W + T_{3i}$ (e.g., $d_{\tilde{u}_L} = \frac{1}{2} - \frac{1}{6}\tan^2\theta_W$, $d_{\tilde{e}_R} = -\tan^2\theta_W$), and $\xi_0 = m_0/m_{1/2}$ $= 0, 1/\sqrt{3}$. The coefficients c_i can be calculated numerically in terms of the low-energy gauge couplings, and are given in Table I[2] for $\alpha_3(M_Z) = 0.118 \pm 0.008$. In the table we also give $c_{\tilde{g}} = m_{\tilde{g}}/m_{1/2}$. Note that these values are smaller than what is obtained in the minimal SU(5) supergravity model [where $c_{\tilde{g}} = 2.90$ for $\alpha_3(M_Z) = 0.118$] and therefore the numerical relations between the gluino mass and the neutralino masses are different in that model. In the table we also show the resulting values for a_i, b_i for the central value of $\alpha_3(M_Z)$.

The "average" squark mass, $m_{\tilde{q}} \equiv \frac{1}{8}(m_{\tilde{u}_L} + m_{\tilde{u}_R} + m_{\tilde{d}_L} + m_{\tilde{d}_R} + m_{\tilde{c}_L} + m_{\tilde{c}_R} + m_{\tilde{s}_L} + m_{\tilde{s}_R}) = (m_{\tilde{g}}/c_{\tilde{q}})\ (\bar{c}_{\tilde{q}} + \xi_0^2)^{1/2}$, with $\bar{c}_{\tilde{q}}$ given in Table I, is determined to be

TABLE I. The value of the c_i coefficients appearing in Eq. (9), the ratio $c_{\tilde{g}} = m_{\tilde{g}}/m_{1/2}$, and the average squark coefficient $\bar{c}_{\tilde{q}}$, for $\alpha_3(M_Z) = 0.118 \pm 0.008$. Also shown are the a_i, b_i coefficients for the central value of $\alpha_3(M_Z)$ and both supersymmetry-breaking scenarios (T: moduli, S: dilaton). The results apply as well to the second-generation squark and slepton masses.

i	c_i (0.110)	c_i (0.118)	c_i (0.126)	
$\tilde{\nu}$, $\tilde{e}_L$	0.406	0.409	0.413	
$\tilde{e}_R$	0.153	0.153	0.153	
$\tilde{u}_L$, $\tilde{d}_L$	3.98	4.41	4.97	
$\tilde{u}_R$	3.68	4.11	4.66	
$\tilde{d}_R$	3.63	4.06	4.61	
$c_{\tilde{g}}$	1.95	2.12	2.30	
$\bar{c}_{\tilde{q}}$	3.82	4.07	4.80	
i	$a_i(T)$	$b_i(T)$	$a_i(S)$	$b_i(S)$
$\tilde{e}_L$	0.302	+1.115	0.406	+0.616
$\tilde{e}_R$	0.185	+2.602	0.329	+0.818
$\tilde{\nu}$	0.302	−2.089	0.406	−1.153
$\tilde{u}_L$	0.991	−0.118	1.027	−0.110
$\tilde{u}_R$	0.956	−0.016	0.994	−0.015
$\tilde{d}_L$	0.991	+0.164	1.027	+0.152
$\tilde{d}_R$	0.950	−0.033	0.989	−0.030

[2]These are renormalized at the scale M_Z. In a more accurate treatment, the c_i would be renormalized at the physical sparticle mass scale, leading to second-order shifts on the sparticle masses.

$$m_{\tilde{q}} = \begin{cases} (1.00, 0.95, 0.95) m_{\tilde{g}} & \text{moduli,} \\ (1.05, 0.99, 0.98) m_{\tilde{g}} & \text{dilaton} \end{cases} \tag{10}$$

for $\alpha_3(M_Z) = 0.110, 0.118, 0.126$ (the dependence on $\tan\beta$ is small). The squark splitting around the average is $\approx 2\%$.

The first- and second-generation squark and slepton masses are plotted in Fig. 2. The thickness and straightness of the lines shows the small $\tan\beta$ dependence, except for $\tilde{\nu}$. The results do not depend on the sign of μ, except to the extent that some points in parameter space are not allowed for both signs of μ: the $\mu < 0$ lines start off at larger mass values. Note that

$$\text{moduli:} \begin{cases} m_{\tilde{e}_R} \approx 0.18 m_{\tilde{g}}, \\ m_{\tilde{e}_L} \approx 0.30 m_{\tilde{g}}, \\ m_{\tilde{e}_R} / m_{\tilde{e}_L} \approx 0.61 , \end{cases}$$

$$\text{dilaton:} \begin{cases} m_{\tilde{e}_R} \approx 0.33 m_{\tilde{g}}, \\ m_{\tilde{e}_L} \approx 0.41 m_{\tilde{g}}, \\ m_{\tilde{e}_R} / m_{\tilde{e}_L} \approx 0.81 . \end{cases} \tag{11}$$

The third-generation squark and slepton masses cannot be determined analytically. These are shown in Fig. 3,

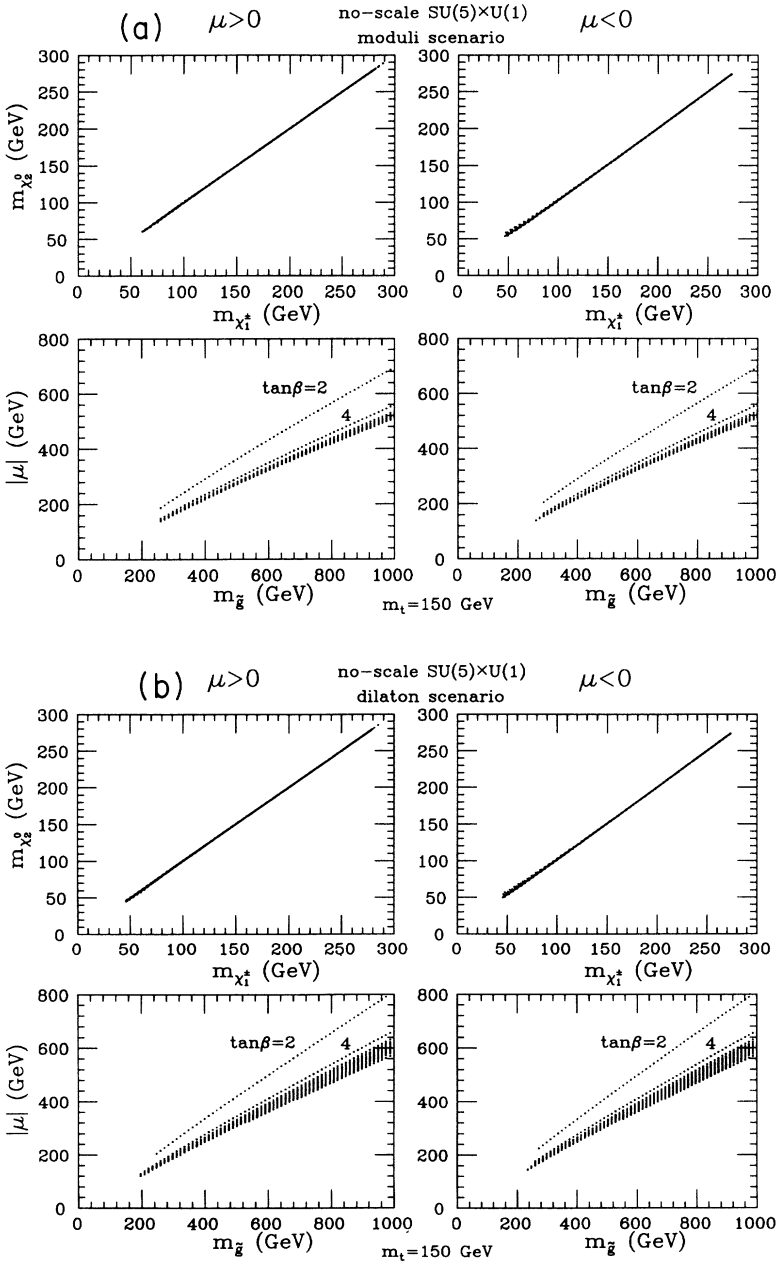

FIG. 1. The correlation between the lightest chargino mass $m_{\chi_1^\pm}$ and the next-to-lightest neutralino mass $m_{\chi_2^0}$ (top row) for both signs of μ, $m_t = 150$ GeV, and (a) the moduli and (b) dilaton scenarios. Also shown (bottom row) is the absolute value of the Higgs-mixing parameter μ versus the gluino mass. Two values of $\tan\beta$ are singled out, larger ones tend to accumulate and are not individually discernible in the figure.

and exhibit a large variability for fixed $m_{\tilde{g}}$ because of the tanβ dependence in the off-diagonal element of the corresponding 2×2 mass matrices. The lowest values of the $\tilde{t}_1$ mass go up with m_t and can be as low as

$$m_{\tilde{t}_1} \gtrsim \begin{cases} 160, 170, 190 (155, 150, 170) \text{ GeV} & \text{moduli,} \\ 88, 112, 150, (92, 106, 150) \text{ GeV} & \text{dilaton} \end{cases} \quad (12)$$

for $m_t = 130, 150, 170$ GeV and $\mu > 0 (\mu < 0)$.

The one-loop corrected lightest *CP*-even (h) and *CP*-odd (A) Higgs-boson masses are shown in Fig. 4. Following the methods of Ref. [34] we have determined that the LEP lower bound on m_h becomes $m_h \gtrsim 60$ GeV. The largest value of m_h depends on m_t; we find

$$m_h < \begin{cases} 106, 115, 125 \text{ GeV} & \text{moduli,} \\ 107, 117, 125 \text{ GeV} & \text{dilaton} \end{cases} \quad (13)$$

for $m_t = 130, 150, 170$ GeV. Note that even though m_A can be fairly light, we always get $m_A > m_h$, in agreement with a general theorem to this effect in supergravity theories [35]. This result also implies that the channel $e^+e^- \to hA$ at LEP I is not kinematically allowed in this model.

The computation of the neutralino relic density (following the methods of Refs. [36,37]) shows that $\Omega_\chi h_0^2 \lesssim 0.25 (0.90)$ in the moduli (dilaton) scenarios. This implies that in these models the cosmologically interesting values $\Omega_\chi h_0^2 \lesssim 1$ occur quite naturally. These results are in good agreement with the observational upper bound on $\Omega_\chi h_0^2$ [38].

As we have discussed, in the scenarios we consider all sparticle masses scale with the gluino mass, with a mild tanβ dependence (except for the third-generation squark and slepton masses). In Table II we collect the approximate proportionality coefficients to the gluino mass for each sparticle mass (not including the third-generation squarks and sleptons). From this table one can (approxi-

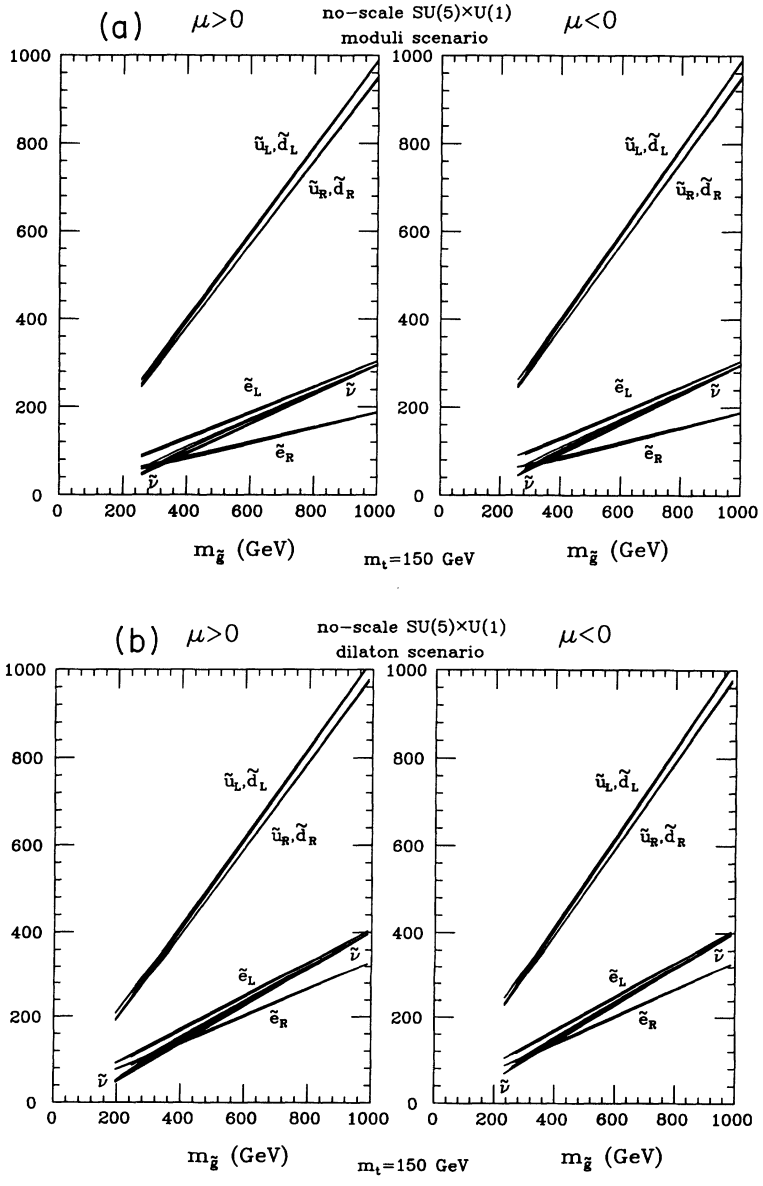

FIG. 2. The first-generation squark and slepton masses as a function of the gluino mass, for both signs of μ, $m_t = 150$ GeV, and (a) the moduli and (b) dilaton scenarios. The same values apply to the second generation. The thickness of the lines and their deviation from linearity are because of the small tanβ dependence.

mately) translate any bounds on a given sparticle mass on bounds on all the other sparticle masses.

D. Special cases

1. *Strict no-scale case*

We now impose the additional constraint $B(M_U)=0$ to be added to Eq. (2), and obtain the so-called strict no-scale case [10]. Since $B(M_Z)$ is determined by the radiative electroweak symmetry-breaking conditions, this added constraint needs to be imposed in a rather indirect way. That is, for given $m_{\tilde{g}}$ and m_t values, we scan the possible values of $\tan\beta$ looking for cases where $B(M_U)=0$. The most striking result is that solutions exist *only* for $m_t \lesssim 135$ GeV if $\mu>0$ and for $m_t \gtrsim 140$ GeV if $\mu<0$. That is, the value of m_t *determines* the sign of μ. Furthermore, for $\mu<0$ the value of $\tan\beta$ is determined uniquely as a function of m_t and $m_{\tilde{g}}$, whereas for $\mu>0$, $\tan\beta$ can be double valued for some m_t range which includes $m_t=130$ GeV.

All the mass relationships deduced in the previous subsection apply here as well. The $\tan\beta$ spread that some of them have will be much reduced though. The most noticeable changes occur for the quantities which depend most sensitively on $\tan\beta$, such as the Higgs-boson masses. Figure 5 of Ref. [1] shows that the one-loop-corrected lightest Higgs-boson mass is largely determined by m_t, with a weak dependence on $m_{\tilde{g}}$. Moreover, for $m_t \lesssim 135$ GeV $\Longrightarrow \mu>0$, $m_h \lesssim 105$ GeV; whereas for $m_t \gtrsim 140$ GeV $\Longrightarrow \mu<0$, $m_h \gtrsim 100$ GeV. Therefore, in the strict no-scale

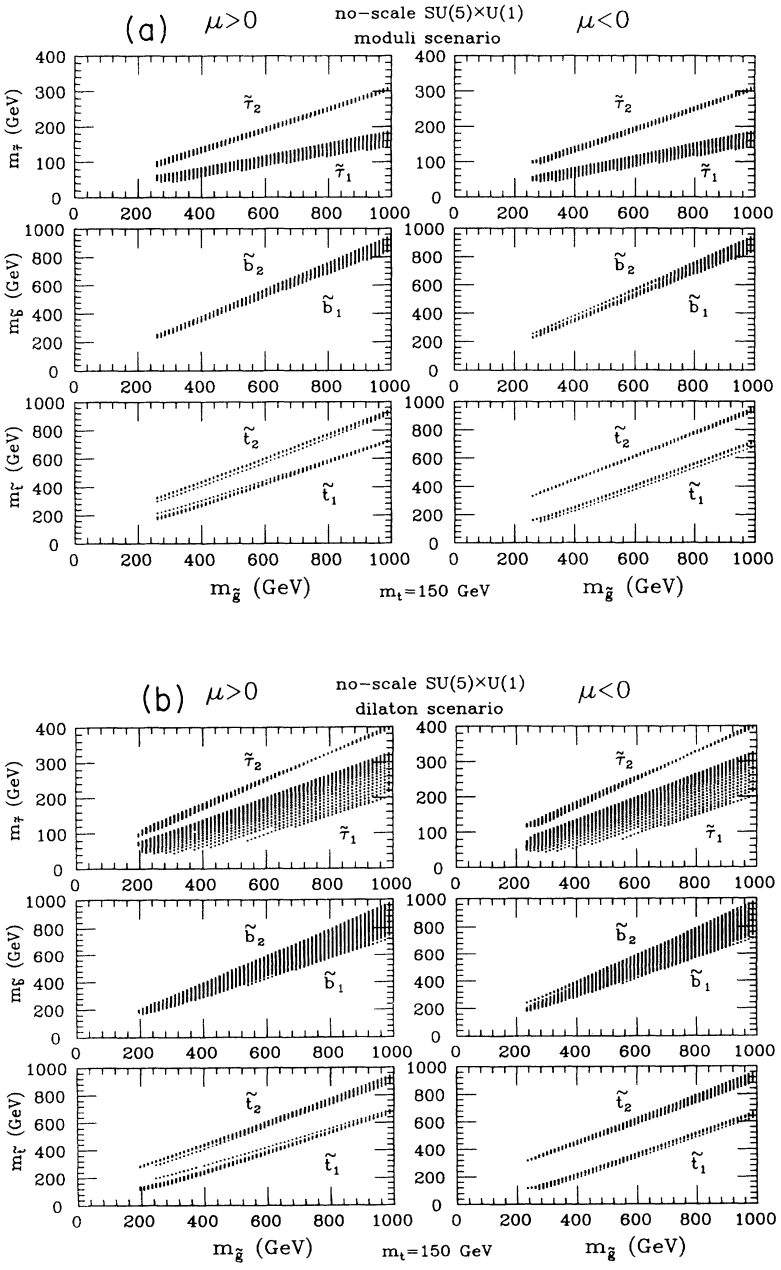

FIG. 3. The $\tilde{\tau}_{1,2}$, $\tilde{b}_{1,2}$, and $\tilde{t}_{1,2}$ masses vs the gluino mass for both signs of μ, $m_t=150$ GeV, and (a) the moduli and (b) dilaton scenarios. The variability in the $\tilde{\tau}_{1,2}$, $\tilde{b}_{1,2}$, and $\tilde{t}_{1,2}$ masses is because of the off-diagonal elements of the corresponding mass matrices.

case, once the top-quark mass is measured, we will know the sign of μ and whether m_h is above or below 100 GeV.

2. *Special dilaton scenario case*

In the analysis described above, the radiative electroweak breaking conditions were used to determine the magnitude of the Higgs mixing term μ at the electroweak scale. This quantity is ensured to remain light as long as the supersymmetry-breaking parameters remain light. In a fundamental theory this parameter should be calculable and its value used to determine the Z-boson mass. From this point of view it is not clear that the natural value of μ should be light. In specific models one can obtain such

TABLE II. The approximate proportionality coefficients to the gluino mass, for the various sparticle masses in the two supersymmetry breaking scenarios considered. The $|\mu|$ coefficients apply for $m_t = 150$ GeV only.

	Moduli	Dilaton
$\tilde{e}_R, \tilde{\mu}_R$	0.18	0.33
$\tilde{\nu}$	0.18–0.30	0.33–0.41
$2\chi_1^0, \chi_2^0, \chi_1^\pm$	0.28	0.28
$\tilde{e}_L, \tilde{\mu}_L$	0.30	0.41
$\tilde{q}$	0.97	1.01
$\tilde{g}$	1.00	1.00
$\lvert\mu\rvert$	0.5–0.7	0.6–0.8

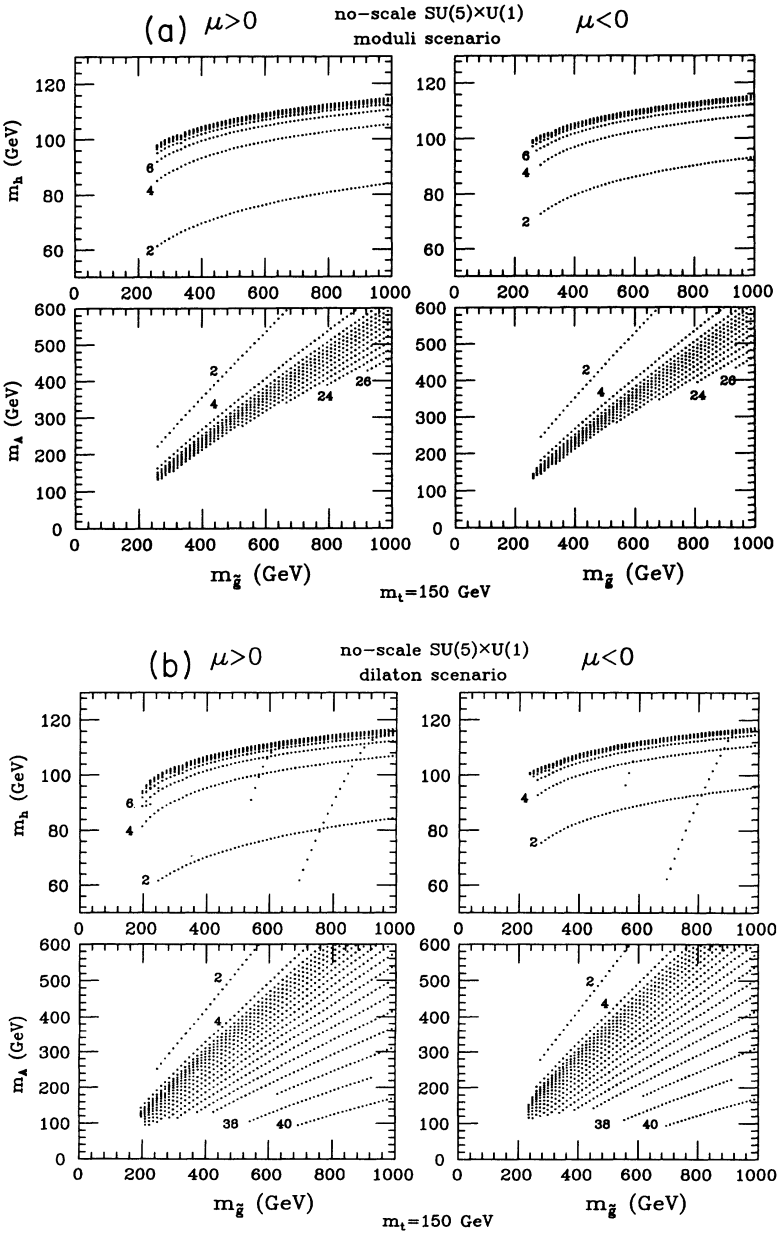

FIG. 4. The one-loop corrected h and A Higgs-boson masses versus the gluino mass for both signs of μ, $m_t = 150$ GeV, and (a) the moduli and (b) dilaton scenarios. Representative values of tanβ are indicated.

values by invoking nonrenormalizable interactions [39,40,5]. Another contribution to this quantity is generically present in string supergravity models [41,40,12]. The general case with contributions from both sources has been effectively dealt with in the previous section. If one assumes that only supergravity-induced contributions to μ exist, then it can be shown that the B parameter at the unification scale is also determined [12,13],

$$B(M_U)=2m_0=\frac{2}{\sqrt{3}}m_{1/2}\ , \tag{14}$$

which is to be added to the set of relations in Eq. (1). This new constraint effectively determines $\tan\beta$ for given m_t and $m_{\tilde{g}}$ values and makes this restricted version of the model highly predictive [17].

It can be shown [17] that only solutions with $\mu<0$ exist. A numerical iterative procedure allows us to determine the value of $\tan\beta$ which satisfies Eq. (14), from the calculated value of $B(M_Z)$. We find that

$$\tan\beta\approx 1.57-1.63, 1.37-1.45, 1.38-1.40$$
$$\text{for } m_t=130, 150, 155 \text{ GeV} \tag{15}$$

is required. Since $\tan\beta$ is so small ($m_h^{\text{tree}}\approx 28-41$ GeV), a significant one-loop correction to m_h is required to increase it above its experimental lower bound of ≈ 60 GeV [34]. This requires the largest possible top-quark masses and a not-too-small squark mass. However, perturbative unification imposes an upper bound on m_t for a given $\tan\beta$ [32], which in this case implies [18]

$$m_t \lesssim 155 \text{ GeV}\ , \tag{16}$$

which limits the magnitude of m_h:

$$m_h \lesssim 74, 87, 91 \text{ GeV} \quad \text{for } m_t=130, 150, 155 \text{ GeV}\ . \tag{17}$$

In Table III we give the range of sparticle and Higgs-boson masses that are allowed in this case.

TABLE III. The range of allowed sparticle and Higgs-boson masses in the special dilaton scenario. The top-quark mass is restricted to be $m_t<155$ GeV. All masses in GeV.

m_t	130	150	155
$\tilde{g}$	335–1000	260–1000	640–1000
χ_1^0	38–140	24–140	90–140
$\chi_2^0,\chi_1^\pm$	75–270	50–270	170–270
$\tan\beta$	1.57–1.63	1.37–1.45	1.38–1.40
h	61–74	64–87	84–91
$\tilde{l}$	110–400	90–400	210–400
$\tilde{q}$	335–1000	260–1000	640–1000
A,H,H^+	>400	>400	>970

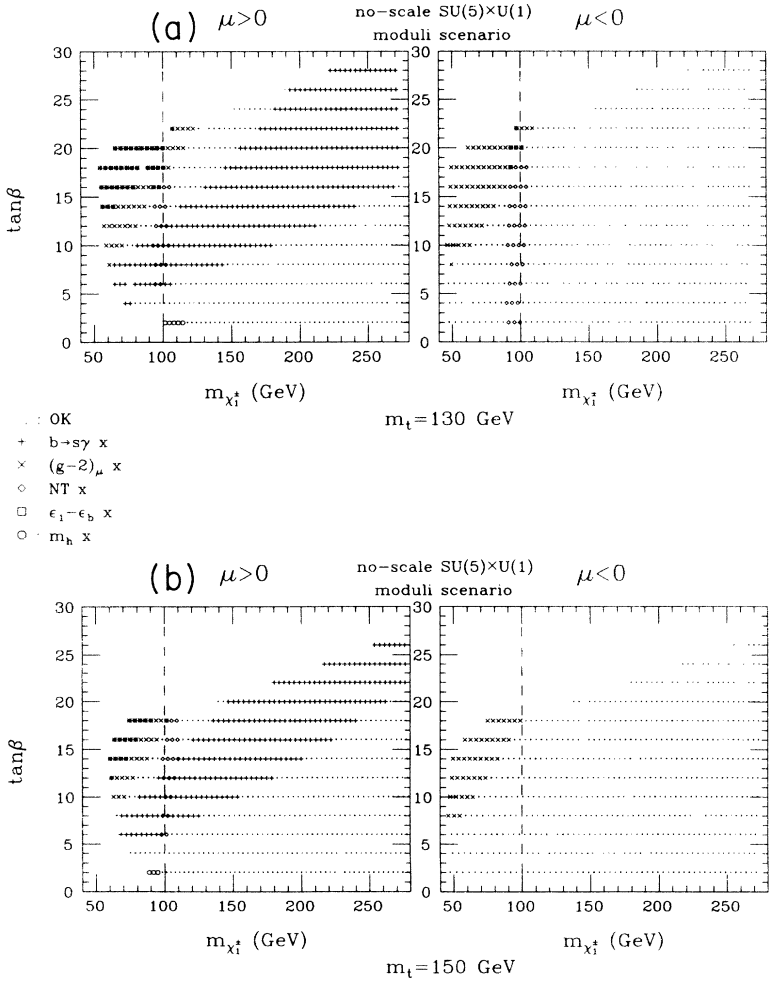

FIG. 5. The parameter space for no-scale SU(5)×U(1) supergravity (moduli scenario) in the $(m_{\chi_1^\pm},\tan\beta)$ plane for (a) $m_t=130$ GeV, (b) $m_t=150$ GeV, (c) $m_t=170$ GeV, and (d) $m_t=180$ GeV. The periods indicate points that passed all constraints, the plusses fail the $B(b\to s\gamma)$ constraint, the crosses fail the $(g-2)_\mu$ constraint, the diamonds fail the neutrino telescopes (NT) constraint, the squares fail the $\epsilon_1-\epsilon_b$ constraint, and the octagons fail the updated Higgs-boson mass constraint. The reference dashed line highlights $m_{\chi_1^\pm}=100$ GeV, which is the direct reach of LEP II for chargino masses. Note that when various symbols overlap a more complex symbol is obtained.

III. CONSTRAINTS ON PARAMETER SPACE

In this section we describe the experimental constraints which have been applied to the points in the basic parameter space described in Sec. II. Each of these constraints leads to an excluded area in the $(m_{\chi_1^\pm}, \tan\beta)$ plane for a fixed value of m_t. Since all sparticle masses scale with $m_{1/2}$, the lightest chargino mass is as good a choice as any other one, and has the advantage of being readily measurable. Our choices for m_t, i.e., $m_t = 130, 150, 170, 180$ GeV are motivated by the direct lower limit on the top-quark mass from Tevatron searches ($m_t > 131$ GeV [42]) and by the indirect estimates of the mass from fits to the electroweak data ($m_t = 140 \pm 20$ GeV [29,30]). The effect of each of the constraints is denoted by a particular symbol on the parameter space plots in Figs. 5–8 for the various scenarios under consideration. In all these figures there is an eye-guiding vertical dashed line which corresponds to $m_{\chi_1^\pm} = 100$ GeV. The purpose of Fig. 7 is to show where such a line lies in the $(m_g, \tan\beta)$ plane. Kinematically speaking, the weakly interacting sparticles (i.e., charginos) are more accessible than the strongly interacting ones (i.e., gluino and squarks).

A. $b \to s\gamma$

The rare radiative flavor-changing-neutral-current (FCNC) $b \to s\gamma$ decay has been observed by the CLEOII Collaboration in the 95% C.L. range $B(b \to s\gamma) = (0.6\text{–}5.4) \times 10^{-4}$ [43]. Since large enhancements and suppressions of $B(b \to s\gamma)$, relative to the standard model value, can occur in SU(5)×U(1) supergravity, the above allowed interval can be quite restrictive [19,20] (see also Ref. [44,45]). The results of the calculation in the moduli and dilaton scenarios are given in Refs. [19,20]. In both scenarios there exists a significant region of parameter space where $B(b \to s\gamma)$ is highly suppressed [19,20]. The points in parameter space which are excluded at the 95% C.L. are denoted by pluses (+) in Figs. 5 and 6 for the moduli and dilaton scenarios, respectively, and for the four chosen values of m_t. The strict no-scale scenario [see Fig. 8(a)] is also constrained in this fashion, although only for $m_t = 130, 150$ GeV. The special dilaton scenario is not constrained by $B(b \to s\gamma)$ [see Fig. 8(b)] because of the small values of $\tan\beta$ required in this case. Note that the constraints are generally much stricter for $\mu > 0$.

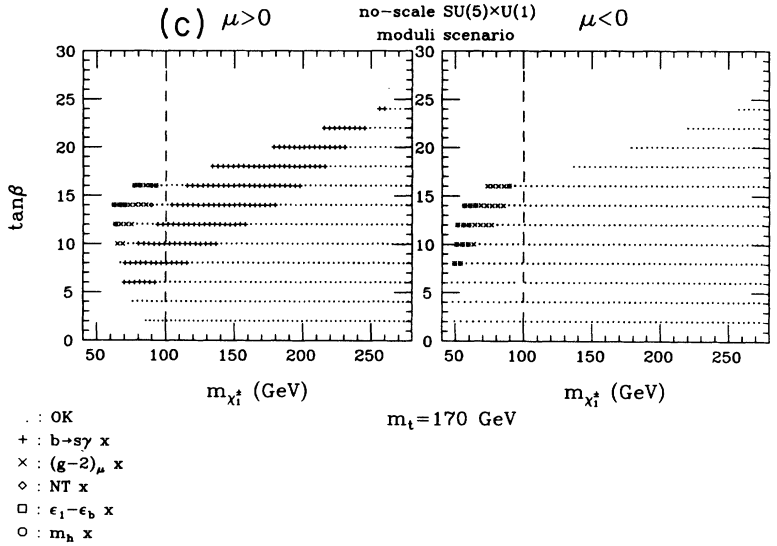

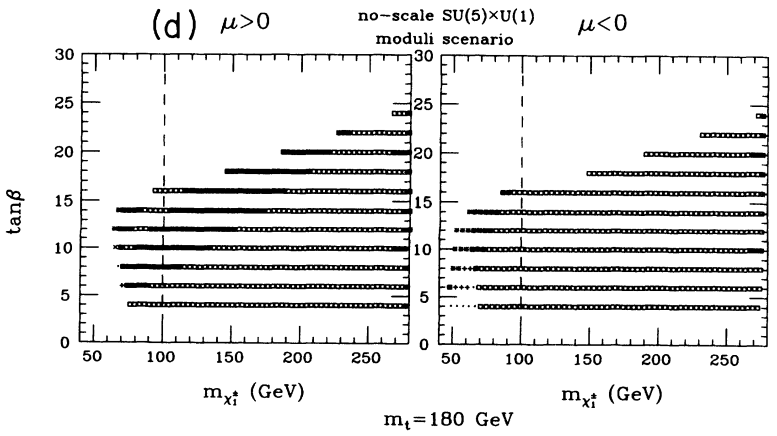

FIG. 5. (*Continued*).

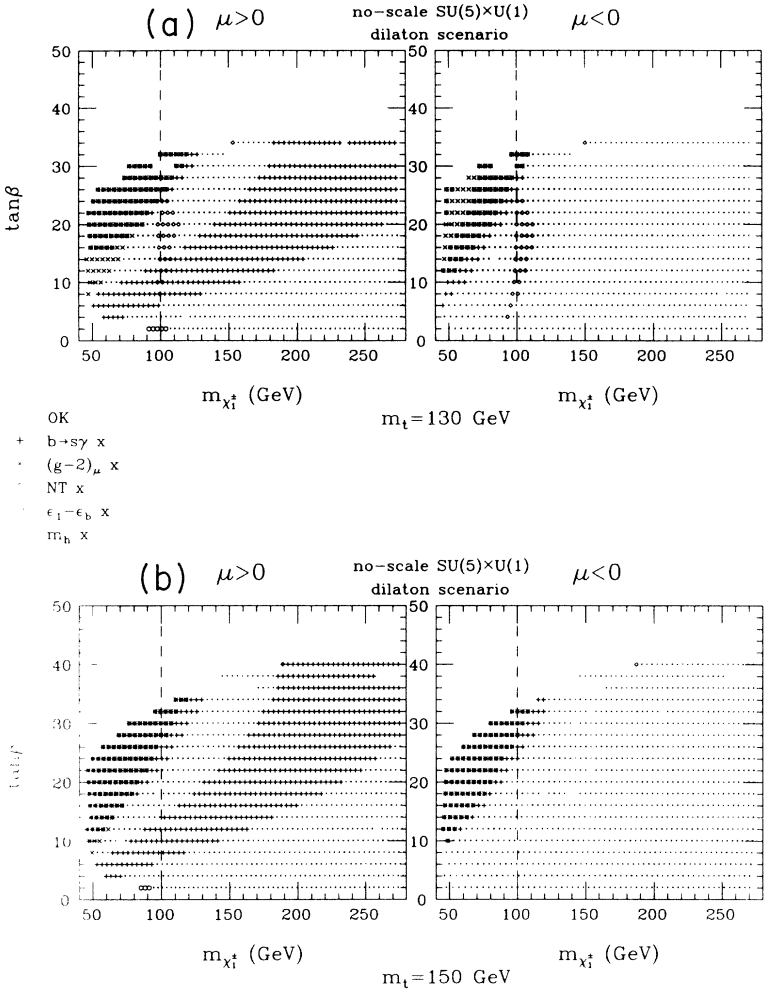

FIG. 6. The parameter space for no-scale SU(5)×U(1) supergravity (dilaton scenario) in the $(m_{\chi_1^\pm}, \tan\beta)$ plane for (a) $m_t = 130$ GeV, (b) $m_t = 150$ GeV, (c) $m_t = 170$ GeV, and (d) $m_t = 180$ GeV. The periods indicate points that passed all constraints, the pluses fail the $B(b \to s\gamma)$ constraint, the crosses fail the $(g-2)_\mu$ constraint, the diamonds fail the neutrino telescopes (NT) constraint, the squares fail the $\epsilon_1 - \epsilon_b$ constraint, and the octagons fail the updated Higgs-boson mass constraint. The reference dashed line highlights $m_{\chi_1^\pm} = 100$ GeV, which is the direct reach of LEP II for chargino masses. Note that when various symbols overlap a more complex symbol is obtained.

B. $(g-2)_\mu$

The supersymmetric contributions to $a_\mu = \frac{1}{2}(g-2)_\mu$ in SU(5)×U(1) supergravity have been recently computed in Ref. [21], and have been compared with the presently allowed 95% C.L. interval $-13.2\times10^{-9} < a_\mu^{\rm SUSY} < 20.8 \times 10^{-9}$. In this paper it was noted that a contribution to a_μ, which is roughly proportional to $\tan\beta$, leads to enhancements which can easily make $a_\mu^{\rm SUSY}$ run in conflict with the present experimental bounds. The points in parameter space which are excluded at the 95% C.L. are denoted by crosses (×) in Figs. 5 and 6 for the moduli and dilaton scenarios, respectively, and for the four chosen values of m_t. As expected, the $(g-2)_\mu$ constraint has a similar effect for the two signs of μ, and exclude the larger values of $\tan\beta$ which are allowed for chargino masses up to about 100 GeV. The constraint appears less effective for $m_t = 170, 180$ GeV (i.e., there are fewer crosses), but this is just because for the larger values of m_t, $\tan\beta$ is cutoff at smaller values. The strict no-scale scenario [see Fig. 8(a)] is also constrained in this fashion, although only for $m_t = 130, 150$ GeV. The special dilaton scenario is not constrained by $(g-2)_\mu$ [see Fig. 8(b)] because of the small values of $\tan\beta$ required in this case (i.e., $\tan\beta < 1.64$).

C. Neutrino telescopes

Neutralinos in the galactic halo which are gravitationally captured by the Sun or Earth [46,47], annihilate into all possible ordinary particles, and the cascade decays of these particles produce high-energy neutrinos as one of several end products. These neutrinos can then travel from the Sun or Earth cores to the vicinity of underground detectors ("neutrino telescopes"), and interact with the rock underneath producing detectable upwardly moving muons. The calculation of the upwardly moving muon fluxes induced by the neutrinos from the Sun and Earth in SU(5)×U(1) supergravity has been performed in Ref. [24]. The present experimental constraints from "neutrino telescopes" on the parameter space are quite weak, as evidenced by the few excluded points in Figs. 5 and 6 (denoted by diamonds "◇"). In fact, the Kamiokande upper bound from the Earth capture is only useful to exclude regions of the parameter space with $m_\chi \approx m_{\rm Fe}$ due to the kinematic enhancement in the capture rate. Because of the weakness of this constraint, the effect has not been calculated for the special scenarios in Fig. 8. Nonetheless, future improved sensitivity in underground muon detection rates should make this constraint

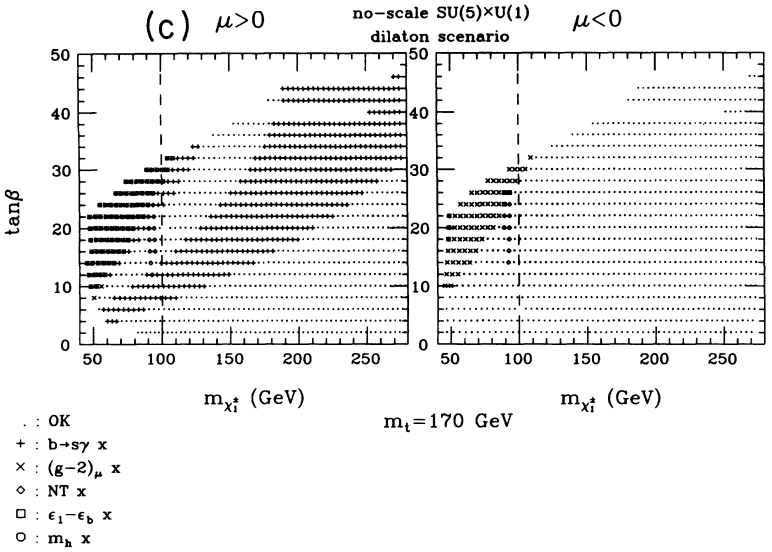

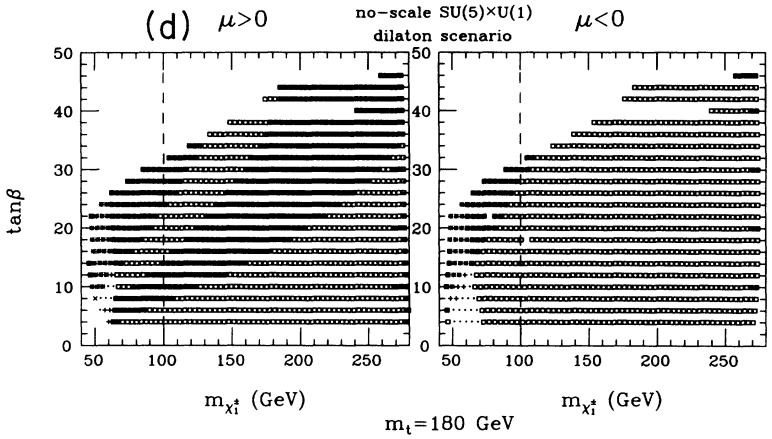

FIG. 6. (*Continued*).

rather important, if neutralinos indeed constitute a significant portion of the dark galactic halo.

D. Updated precision electroweak tests

Among the various schemes to parametrize the electroweak vacuum polarization corrections [48–51], we choose the so-called ϵ scheme [52,53] which is more suitable to the electroweak precision tests of the MSSM [54] and a class of supergravity models [22]. There are two ϵ schemes. The original scheme [52] was considered in our previous analyses [22,20], where $\epsilon_{1,2,3}$ are defined from a basic set of observables Γ_l, A_{FB}^l and M_W/M_Z. Because of the large m_t-dependent vertex corrections to Γ_b, the $\epsilon_{1,2,3}$ parameters and Γ_b can be correlated only for a fixed value of m_t. However, in the new ϵ scheme, introduced recently in Ref. [53], the above difficulties are overcome by introducing a new parameter, ϵ_b, to encode the $Z\to b\bar{b}$ vertex corrections. The four ϵ's are now defined from an enlarged set of Γ_l, Γ_b, A_{FB}^l and M_W/M_Z without even specifying m_t. Here we use this new ϵ scheme. Experimentally, including all of the latest LEP data (complete 1992 LEP data plus preliminary 1993 LEP data) allows one to determine most accurately the allowed ranges for these parameters [29]:

$$\epsilon_1^{\text{expt}}=(1.8\pm3.1)\times10^{-3}\ ,$$
$$\epsilon_b^{\text{expt}}=(-0.5\pm5.1)\times10^{-3}\ . \tag{18}$$

We only discuss ϵ_1,ϵ_b since only these parameters provide constraints in supersymmetric models at the 90% C.L. [22,25]. The expressions for ϵ_1 and ϵ_b have been discussed in Ref. [23]. Compared with the previous experimental values for the ϵ parameters obtained by including the complete 1992 LEP data [56] (which were used in Ref. [23]) those in Eq. (18) have moved in such a way that the standard model predictions have become in better agreement with LEP data than before [29,30]. In Fig. 9 we present the results of the calculation of ϵ_1 and ϵ_b (as described above) for all the allowed points in SU(5)×U(1) supergravity in both moduli and dilaton scenarios, and for $m_t=130,150,170,180$ GeV. In the figures we include three experimental ellipses representing the $1-\sigma$ (from Ref. [29]), 90% C.L., and 95% C.L. experimental limits obtained from analyzing all of the latest LEP electroweak data. The shift in the experimental data corresponds to a shift in the center point of the ellipses towards larger values of ϵ_1 and smaller values of ϵ_b. As a consequence, at the 90% C.L. there are no constraints from ϵ_b alone

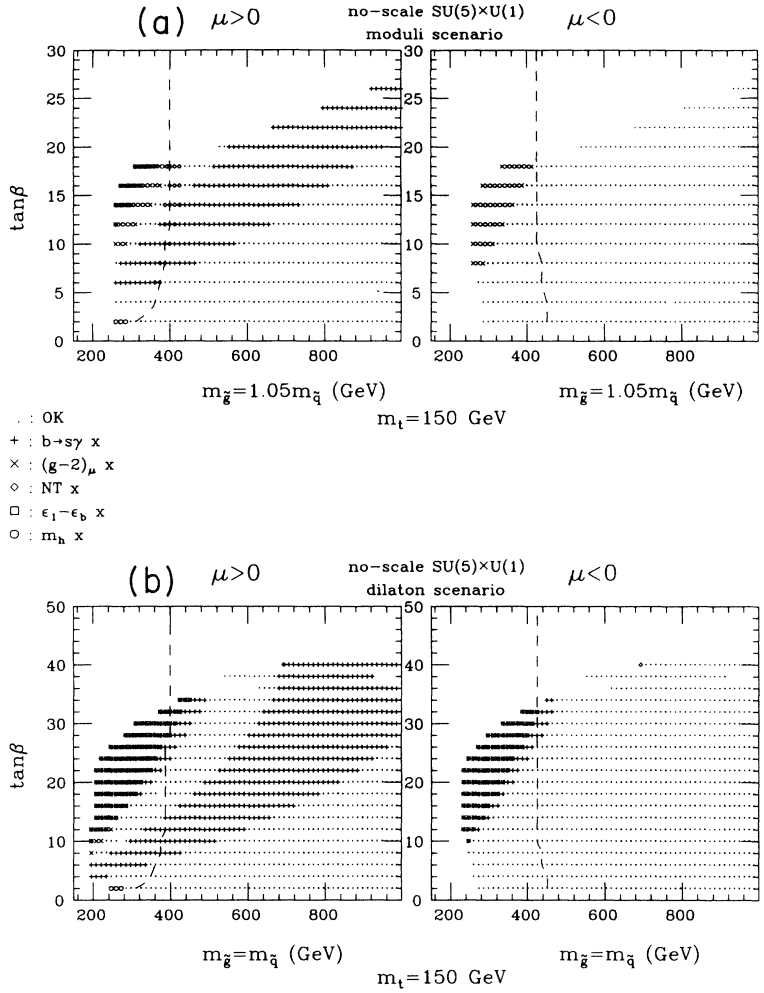

FIG. 7. The parameter space for the moduli and dilaton SU(5)×U(1) supergravity scenarios in the $(m_{\tilde{g}},\tan\beta)$ plane for $m_t=150$ GeV. The meaning of the various symbols is the same as in Figs. 5 and 6. The dashed line marks the contour of $m_{\chi_1^\pm}=100$ GeV (c.f. Figs. 5 and 6) and makes apparent the kinematical disadvantage of searching for the heavier squarks and gluinos, as opposed to the lighter charginos.

(cf. Ref. [23]). Nonetheless, the imposition of the correlated constraint (i.e., the ellipses), is significantly more restrictive than imposing the ϵ_1 constraint by itself.

For both scenarios, the effects of light charginos ($\chi_1^\pm$) and stop squarks ($\tilde{t}_{1,2}$), as described above, are rather pronounced. At the 90% C.L. there are no constraints for $m_t \lesssim 170$ GeV, but for $m_t=180$ GeV only very light charginos ($m_{\chi_1^\pm} \lesssim 70$ GeV) are allowed. Should the top quark be rather heavy, this light-chargino effect would appear to be a sensible explanation.

Now we choose to constrain the parameter space by demanding theoretical predictions which agree with experiment to better than 90% C.L.; i.e., we exclude points in parameter space which are outside the 90% C.L. ellipses in Fig. 9. This constraint entails restrictions for $m_t=180$ GeV only. Note that from our calculations, all $m_t=180$ GeV points are allowed at the 95% C.L. However, more comprehensive analyses [29,30] already exclude $m_t=180$ GeV at the 95% C.L. (i.e., $m_t=140\pm20$ GeV), and thus our restriction is in practice likely to be more statistically significant than can be surmised from our analysis alone. The excluded points in parameter space are shown as squares "□" in Figs. 5(d), 6(d), and 8(a). The effect of this constraint is severe and requires rather light values of the chargino mass. Moreover, such light values of $m_{\chi_1^\pm}$ are very likely to be excluded by other constraints, as the figures show. This means that a "light chargino effect" may not be a viable way out from a possible experimentally heavy top quark.

E. Trileptons

The process of interest is $p\bar{p}\to\chi_2^0\chi_1^\pm X$, where both neutralino and chargino decay leptonically: $\chi_2^0\to\chi_1^0 l^+ l^-$, and $\chi_1^\pm\to\chi_1^0 l^\pm \nu_l$, with $l=e,\mu$. The production cross section proceeds through s-channel W^* exchange and t-channel squark exchange (a small contribution). This signal, first studied in Ref. [57], has been explored in SU(5)×U(1) supergravity in Ref. [25]. The first experimental limits obtained by the D0 [58] and the Collider Detector at Fermilab (CDF) [59,60] Collaborations have been recently announced. The irreducible backgrounds for this process are very small, the dominant one being $p\bar{p}\to W^\pm Z\to(l^\pm\nu_l)(\tau^+\tau^-)$ with a cross section into trileptons of $(\sim1$ pb$)(\frac{2}{9})(0.033)(0.34)^2\sim1$ fb. Much larger "instrumental" backgrounds exist when for example in $p\bar{p}\to Z\gamma$, the photon "converts" and fakes a lepton in the detector; with the present sensitivity, suitable cuts

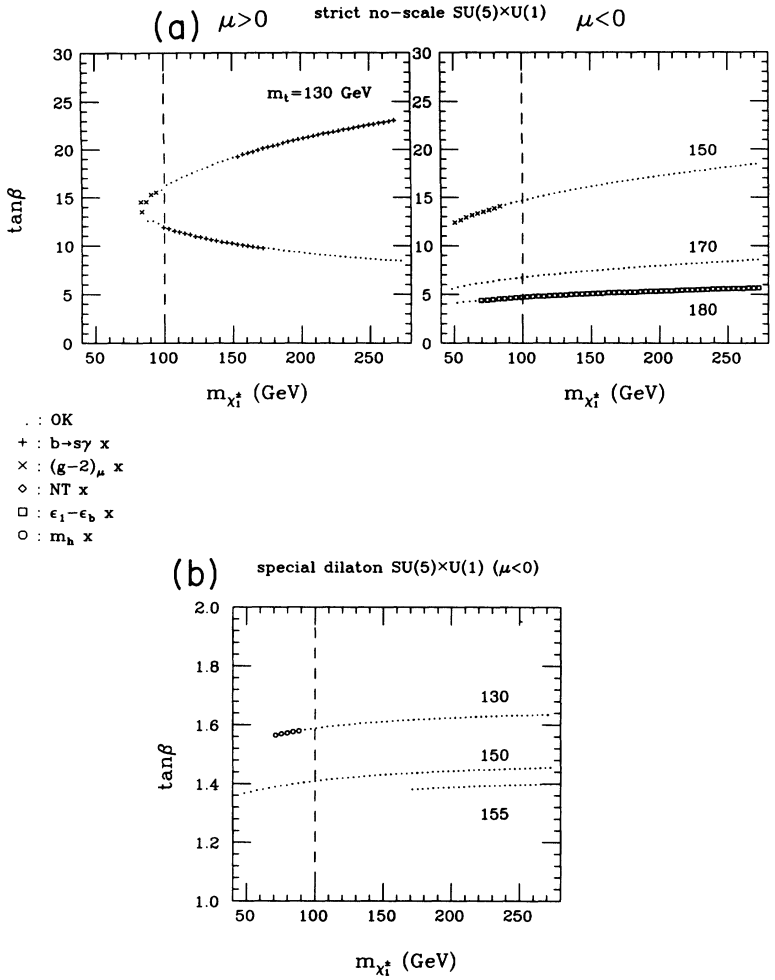

FIG. 8. The parameter space for (a) strict no-scale and (b) special dilaton SU(5)×U(1) supergravity in the $(m_{\chi_1^\pm}, \tan\beta)$ plane. The meaning of the various symbols is the same as in Figs. 5 and 6.

have been designed to reduce this background to acceptable levels [58]. The present experimental limits [58–60] from the Tevatron are rather weak, with sensitivity for $m_{\chi_1^\pm} \lesssim 50$ GeV only [59]. In the case of SU(5)×U(1) supergravity, no points in parameter space are excluded by the present experimental limits. However, with the projected increase in integrated luminosity during 1994, this experimental constraint could soon become relevant, as we discuss in Sec. V A below.

F. Updated Higgs-boson mass limit

The current LEP I lower bound on the standard model (SM) Higgs-boson mass stands at $m_H > 63.8$ GeV [61]. This bound is obtained by studying the process $e^+e^- \to Z^* H$ with subsequent Higgs-boson decay into two jets. The MSSM analogue of this production process leads to a cross section differing just by a factor of $\sin^2(\alpha-\beta)$. In Ref. [34] it was shown that in supergravity models with radiative electroweak symmetry breaking, as is the case of SU(5)×U(1) supergravity, the lightest Higgs boson behaves very much like the standard model Higgs boson. In particular, the $\sin^2(\alpha-\beta)$ factor approaches unity as the supersymmetry mass scale is raised. The branching fraction $B(h \to b\bar{b})$ also approaches the standard model value, although one has to watch out for new supersymmetric decays, most notably $h \to \chi_1^0 \chi_1^0$. In any event, a straightforward procedure to adapt the experimental lower bound on the standard model Higgs-boson mass to the supersymmetric case is described in Ref. [34]. The following condition must be satisfied for allowed points in parameter space [34,62]:

$$f \sin^2(\alpha-\beta) < P(M_H^{\min}/M_Z)/P(m_h/M_Z) , \tag{19}$$

where $M_H^{\min}$ is the experimental lower bound on the standard model Higgs-boson mass (i.e., $M_H^{\min} = 63.8$ GeV), and we have used the fact that the cross sections differ only by the coupling factor $\sin^2(\alpha-\beta)$ and the Higgs-boson mass dependence, which enters through a function P [63]:

$$P(y) = \frac{3y(y^4-8y^2+20)}{\sqrt{4-y^2}} \arccos\left[\frac{y(3-y^2)}{2}\right] - 3(y^4-6y^2+4)\ln y - \tfrac{1}{2}(1-y^2)(2y^4-13y+47) . \tag{20}$$

The determination of the basic parameter space in Sec.

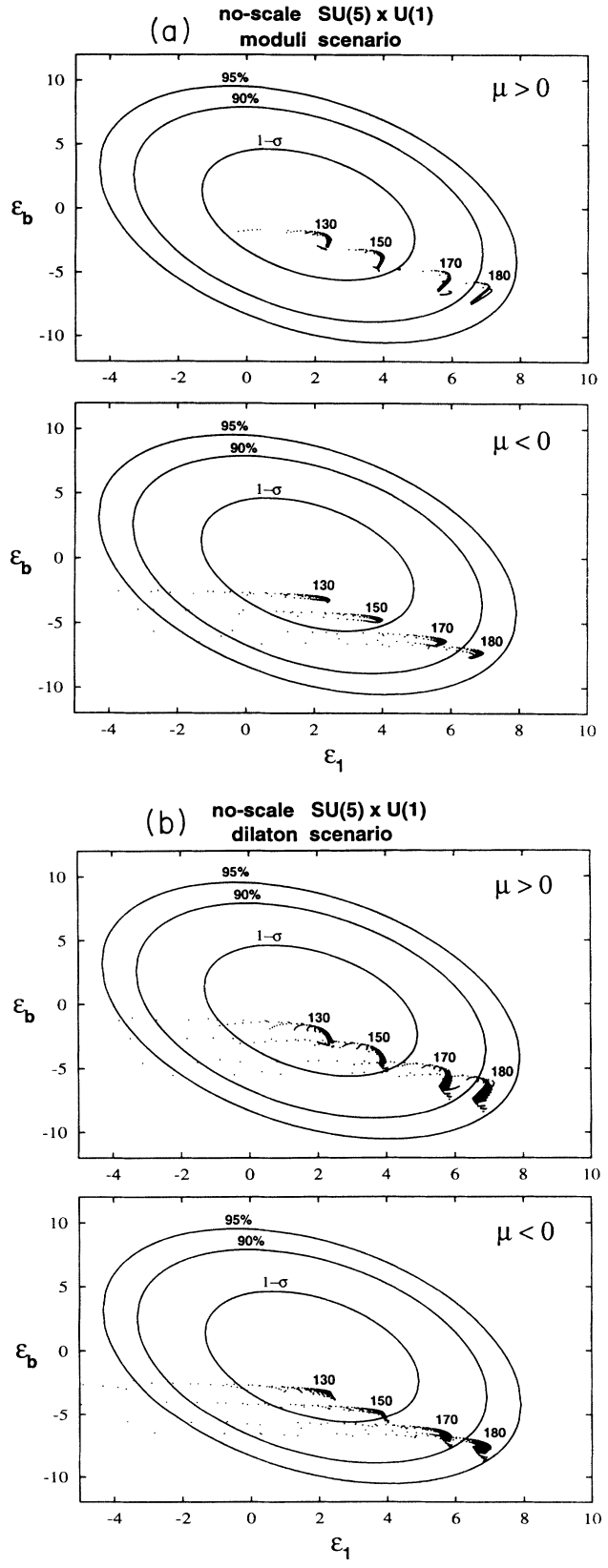

FIG. 9. The correlated values of ϵ_1 and ϵ_b (in units of 10^{-3}) for both signs of μ, $m_t = 130, 150, 170, 180$ GeV, and (a) the moduli and (b) dilaton scenarios. The ellipses represent the 1σ, 90% C.L., and 95% C.L. experimental limits obtained from analyzing all LEP electroweak data.

II, includes the LEP experimental limits on sparticle masses and the experimental limit $M_H^{\min} = 61.3$ GeV. The updated experimental limit of $M_H^{\min} = 63.8$ GeV excludes some further points in parameter space (denoted by octagon symbols in Figs. 5, 6, and 8) for the smallest values of $\tan\beta$ and $m_t = 130, 150$ GeV.

IV. ALLOWED PARAMETER SPACE

The constrained parameter spaces shown in Figs. 5, 6, and 8 show some regularities which are worth pointing out. First, the constraints for $\mu < 0$ are generally weaker than those for $\mu > 0$. It is also clear that the region to the left of the dashed line ($m_{\chi_1^\pm} < 100$ GeV) is rather restricted. This region represents the area of sensitivity at LEP II from direct chargino searches. (LEP II could greatly extend this region through Higgs-boson searches though.)

For $m_t = 180$ GeV things are very constrained. The most important constraint comes from the $\epsilon_1 - \epsilon_b$ ellipses in Fig. 9. Moreover, the remaining allowed points, which require rather light chargino masses ($m_{\chi_1^\pm} \lesssim 70$ GeV), are quite often in conflict with other experimental constraints. The few remaining points in parameter space have $\tan\beta \lesssim 8$ (12) in the moduli (dilaton) scenario. Also, $m_{\chi_1^\pm} \lesssim 68$ (66) GeV and $m_{\chi_1^\pm} \lesssim 65$ (68) GeV for $\mu > 0$ ($\mu < 0$) in the moduli and dilaton scenarios, respectively. For both scenarios, a more sensitive measurement of the $b \to s\gamma$ branching fraction is likely to probe the remaining allowed points for $m_t = 180$ GeV. Also, for $\mu < 0$ in both scenarios, the expected increased sensitivity in trilepton searches is likely to probe about half of the remaining points.

It is interesting to wonder if the present experimental constraints show any preference for particular values of the top-quark mass. To explore this question we carry out the following exercise: we count the number of points in parameter space which are allowed for a fixed value of m_t. We do this in two steps (see Fig. 10): (i) first imposing only the basic theoretical and LEP experimental constraints ("theory + LEP") and (ii) imposing in addition all of the experimental constraints described in Sec. III ("all"). The result in Fig. 10 is interesting. The drop in the "theory + LEP" curves near $m_t = 190$ GeV has been studied in detail (for $m_t = 180, 185, 188, 189$ GeV) and corresponds to encountering a Landau pole in the top-quark-Yukawa coupling below the string scale [32]. The "all" curves show some m_t dependence, although at the moment no marked preference for particular values of m_t is apparent (other than the requirement of $m_t \lesssim 180$ GeV). Note that in spite of the intricate dependence of the sparticle and Higgs-boson masses on the top-quark mass (through the running of the renormalization group equations (RGE's) and the radiative breaking mechanism), the overall size of the parameter space does not depend so critically on m_t.

One can repeat the above exercise to see if any trends

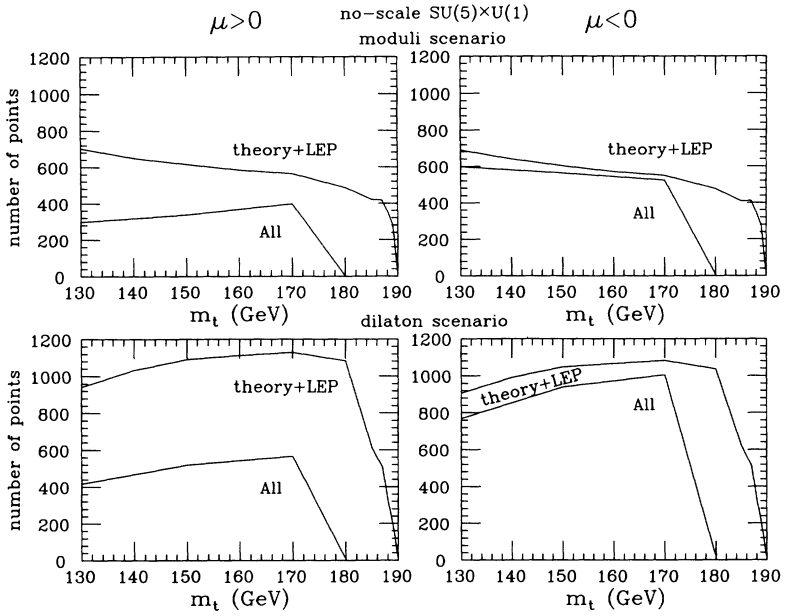

FIG. 10. The number of allowed points in parameter space of the moduli and dilaton SU(5)×U(1) supergravity scenarios as a function of m_t when the basic theoretical and experimental LEP constraints have been imposed ("theory+LEP"), and when all known direct and indirect experimental constraints have been additionally imposed ("all").

on the preferred value of tanβ appear. This time we count the number of allowed points in parameter space for a given value of tanβ, for fixed m_t. The resulting distribution is shown in Fig. 11 for $m_t = 150$ GeV. Qualitatively similar distributions are obtained for other values of m_t. In this case we discover that for $\mu > 0$ there is a significant preference towards the smaller values of tanβ. This result is apparent from Figs. 5 and 6 also, and is mostly a consequence of the $b \to s\gamma$ constraint.

Future improvements in sensitivity on the experimental constraints which we have imposed here, or the advent of new experimental constraints, may sharpen the "predictions" for the preferred values of m_t and tanβ obtained in this statistical exercise.

V. PROSPECTS FOR DIRECT EXPERIMENTAL DETECTION

In this section we consider the still-allowed parameter space, i.e., the points marked by dots in Figs. 5, 6, and 8, and the prospects for their direct experimental detection. In this section we consider only the representative value of $m_t = 150$ GeV.

A. Tevatron

The Tevatron can explore the supersymmetric spectrum through the traditional missing energy signature in the decay of the strongly interacting gluinos and squarks, or through the trilepton signal in the decay of the weakly

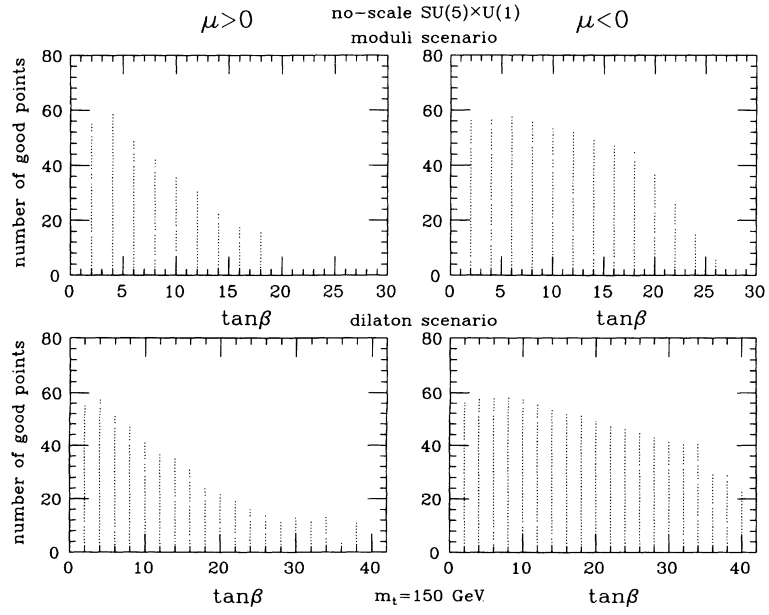

FIG. 11. The number of good points in parameter space in the moduli and dilaton SU(5)×U(1) supergravity scenarios as a function of tanβ for $m_t = 150$ GeV. All known direct and indirect experimental constraints have been imposed. Note that for $\mu > 0$ there is preference for not so large values of tanβ.

interacting charginos and neutralinos. Here we concentrate on the latter signal, whose calculation has been described in Sec. III E. The cross section $\sigma(p\bar{p}\to\chi_1^{\pm}\chi_1^{\pm}\chi_2^0 X)$ (for $\sqrt{s}=1.8$ TeV) is shown in Fig. 12 for $m_t=150$ GeV in the moduli and dilaton scenarios (top row), and shows little variation from one scenario to the other. Moreover, the results for other values of m_t are qualitatively the same and quantitatively quite similar. On the bottom row of Fig. 12 we show the cross section into trileptons, i.e., with the leptonic branching fractions included. The 95% C.L. experimental upper limit from CDF is also indicated.[3] As mentioned above, in the moduli scenario the neutralino leptonic branching fraction can be suppressed for light chargino masses. Note that in the dilaton scenario such suppression is not manifest because of the heavier sparticle mass spectrum. In Fig. 13 we show the analogous results for the strict no-scale and special dilaton scenarios, neither of which show a suppression for light chargino masses.

The present experimental limits from CDF have been obtained by analyzing approximately 18 pb^{-1} of data. By the end of the 1994 run it is expected that each detector will be delivered 75 pb^{-1}, of which CDF should be able to collect say 80%. Therefore, CDF could expect to have about 80 pb^{-1} by the end of the run, which is 4 times the present amount of data. A similar situation is expected from D0. Moreover, the center-of-mass energy will be increased to nearly 2 TeV, which implies a $\approx 30\%$ increase in the chargino-neutralino cross section for 100 GeV charginos. Since tougher cuts will be required to suppress the backgrounds with the increased sensitivity, as a working estimate we have assumed that the new lim-

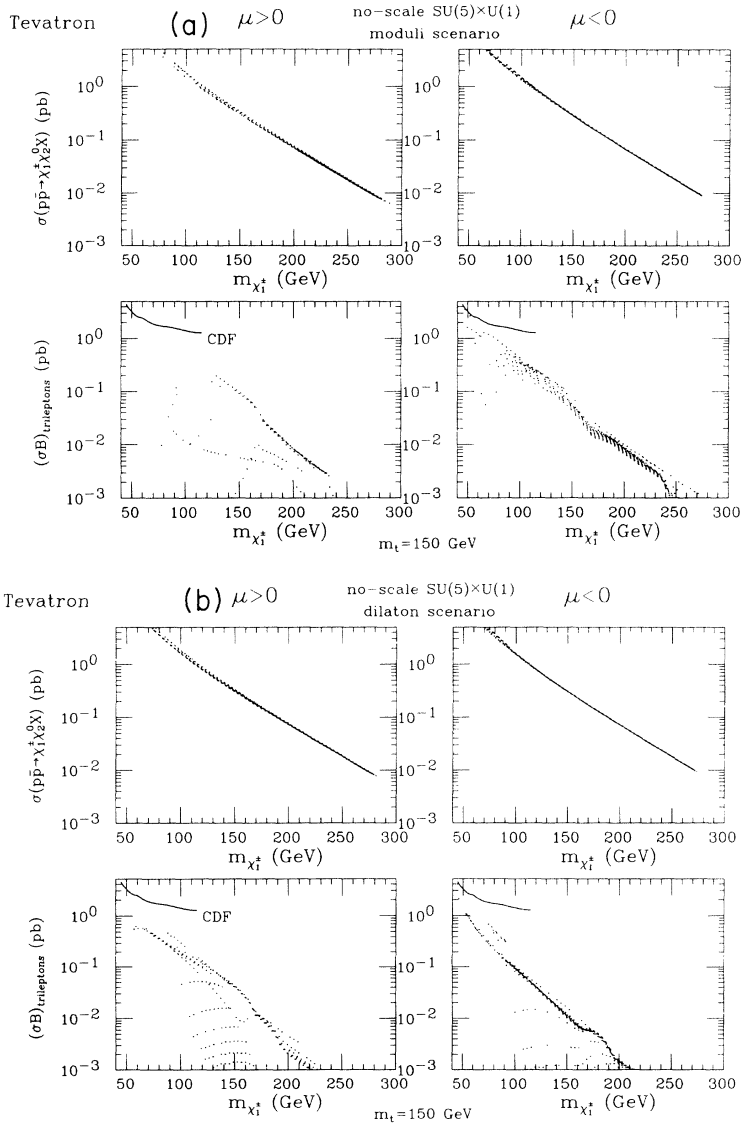

FIG. 12. The cross section $\sigma(p\bar{p}\to\chi_1^{\pm}\chi_2^0 X)$ at the Tevatron (top row) as a function of $m_{\chi_1^{\pm}}$ for $m_t=150$ GeV in (a) the moduli and (b) the dilaton SU(5)×U(1) supergravity scenarios. Also shown (bottom row) is the cross section into trileptons, with the 95% C.L. experimental upper limit from CDF as indicated.

[3]Note that the experimental numbers in Ref. [59] apply to a single channel (i.e., eee, $ee\mu$, $e\mu\mu$, or $\mu\mu\mu$), and need to be multiplied by four to be compared with our predictions for the total $e+\mu$ trilepton rate.

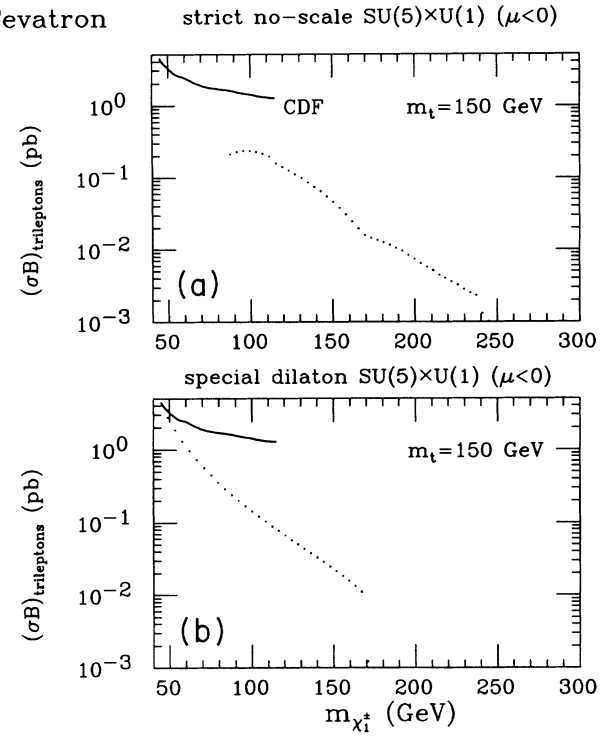

FIG. 13. The trilepton cross section at the Tevatron as a function of $m_{\chi_1^\pm}$ for $m_t=150$ GeV in (a) the strict no-scale and (b) the special dilaton SU(5)×U(1) supergravity scenarios. The 95% C.L. experimental upper limit from CDF is indicated.

its (if no signal is observed) will be down by a factor of 4 from those shown on Fig. 12. We are then able to identify points in the still-allowed parameter space which could be probed by the end of 1994. (The Tevatron will likely not run again until 1997.) These are shown as pluses (+) in Fig. 14 for the moduli and dilaton scenarios. Note that with the increased sensitivity, chargino masses as high as ≈100 GeV could be probed in the moduli scenario. The rates are smaller in the dilaton scenario. Note also that this probe is much more sensitive for $\mu<0$ (see Fig. 12).

Searches for squarks and gluinos at the Tevatron are at kinematical disadvantage in the model under consideration. Indeed, compare the relative position of the dashed vertical line on Fig. 14, with the corresponding line on Fig. 7. The near-future trilepton searches correspond mostly to gluino and squark masses in the range (300–400) GeV, which are likely beyond the direct reach of the Tevatron for the same data set.

B. LEP II

1. Lightest Higgs boson

Perhaps the single most useful piece of information that could come out of LEP II is a measurement of the lightest Higgs-boson mass. Moreover, if the Higgs boson is not observed at LEP II, because of limited statistics or kinematics, still a strong constraint will follow for a large class of supersymmetric models, in particular the ones under consideration here. In Fig. 15 we show the lightest Higgs-boson mass versus $\tan\beta$ for $m_t=150$ GeV in the moduli and dilaton scenarios. Along each vertical line the chargino mass increases from bottom to top. The dotted portions of the lines are already excluded by the various constraints discussed in Sec. III. For $m_t=150$ GeV we find $m_h<118$ GeV. In Fig. 16 we consider the strict no-scale and special dilaton scenarios. Since in these cases the value of $\tan\beta$ is determined (see Fig. 8), the plot is against the chargino mass. In both Figs. 15 and 16 the horizontal line indicates the limit of sensitivity of LEP II for $\sqrt{s}=200$ GeV, as we shortly discuss. First let us note, as pointed out in Ref. [17], that the special dilaton scenario (see Fig. 16) should be completely explored at LEP II (even with $\sqrt{s}=190$ GeV) since $m_t\lesssim 155$ GeV is required in this case (see Sec. II D 2).

In SU(5)×U(1) supergravity, the dominant Higgs-boson production mechanism at LEP II is $e^+e^-\to Z^*\to Zh$. This cross section differs from its standard model counterpart only by a factor of $\sin^2(\alpha-\beta)$. Here we find that generally $\sin^2(\alpha-\beta)>0.96$, in agreement with a general result to this effect [34].[4] The usual analysis of the b-tagged Higgs-boson signal at LEP II also requires the $h\to b\bar{b}$ branching fraction. If we define $f\equiv B(h\to b\bar{b})/B(H_{\rm SM}\to b\bar{b})$, then the expected limit of sensitivity at LEP II, $\sigma(e^+e^-\to Z^*\to ZH_{SM})>0.2$ pb [61] becomes

$$\sigma(e^+e^-\to Z^*\to Zh)\times f>0.2\text{ pb}\ . \tag{21}$$

This size signal is needed to observe a 3σ effect over background with $\mathcal{L}=500$ pb^{-1}. Our results for this quantity are shown in Fig. 17, along with the sensitivity limit in Eq. (21). Note that most points in parameter space accumulate along a well-defined line. This line corresponds to the standard model result. (Deviations from the line are discussed below.) For $\sqrt{s}=200$ GeV, the limit of sensitivity in Eq. (21) translates into $m_h\lesssim 105$ GeV, while for $\sqrt{s}=210$ GeV, $m_h\lesssim 115$ GeV is obtained. From Fig. 17 it would still appear that even with $\sqrt{s}=210$ GeV, some points in parameter space for $m_t=150$ GeV would remain unreachable. However, detailed studies [61] show that for Higgs-boson masses away from the Z pole (here we are interested in $m_h\approx 115-118$ GeV) the limit of sensitivity could be improved to (0.05–0.15) pb, and thus the whole parameter space for $m_t=150$ GeV and all scenarios considered could be explored at LEP II with $\sqrt{s}=210$ GeV. Note that the same conclusion is obtained for $m_t<150$ GeV, since the values of m_h are lower then (e.g., for $m_t=130$ GeV we find $m_h\lesssim 105$ GeV), and even smaller luminosities or beam energies may suffice.

[4] In SU(5)×U(1) supergravity, the $e^+e^-\to hA$ channel is rarely kinematically allowed at LEP II (since $m_A>m_h$) and is further suppressed by the small values of $\cos^2(\alpha-\beta)$.

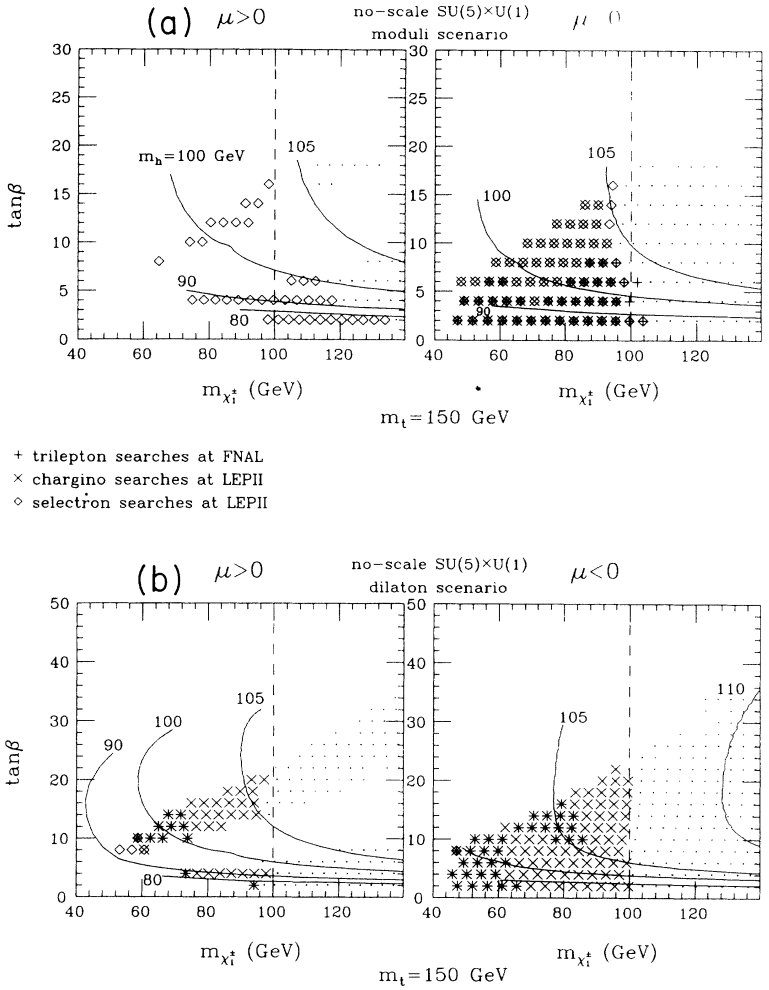

FIG. 14. The still-allowed parameter space in the $(m_{\chi_1^\pm}, \tan\beta)$ plane for $m_t = 150$ GeV in (a) the moduli and (b) the dilaton SU(5)×U(1) supergravity scenarios. The pluses (+) indicate points explorable with near-future trilepton searches at the Tevatron, the crosses (×) will be explorable at LEP II (with $\mathcal{L} = 500$ pb^{-1}) through the mixed mode in chargino pair production, and the diamonds (◇) will be explorable at LEP II (with $\mathcal{L} = 500$ pb^{-1}) through the dilepton mode in selectron pair production. Contours of the lightest one-loop corrected Higgs-boson mass are as indicated (i.e., for $m_h = 80, 90, 100, 105, 110$ GeV). With $\sqrt{s} = 200$ (210) GeV it should be possible to explore at LEP II up to $m_h = 105$ (115) GeV.

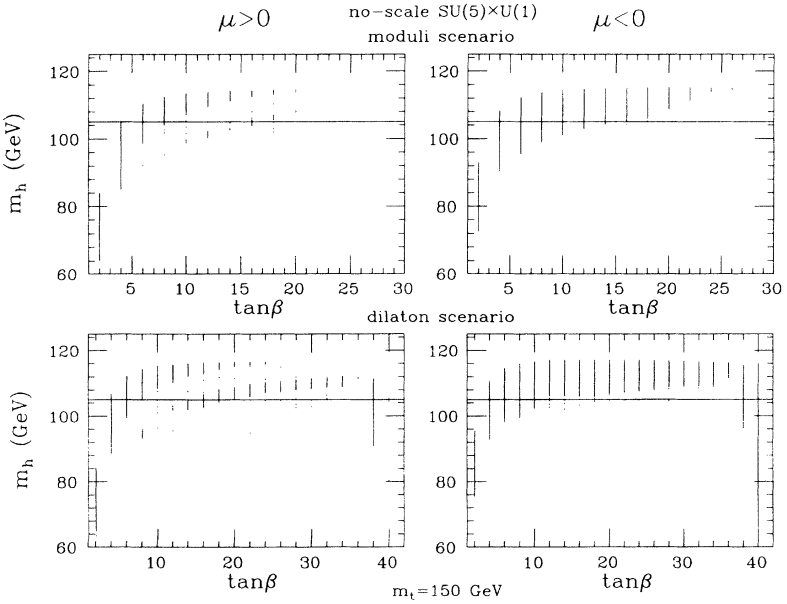

FIG. 15. The lightest one-loop-corrected Higgs-boson mass vs $\tan\beta$ in the moduli and dilaton SU(5)×U(1) supergravity scenarios, for $m_t = 150$ GeV. The dotted portions of the vertical lines indicate excluded ranges of m_h. The horizontal line marks the limit of sensitivity of LEP II with $\sqrt{s} = 200$ GeV.

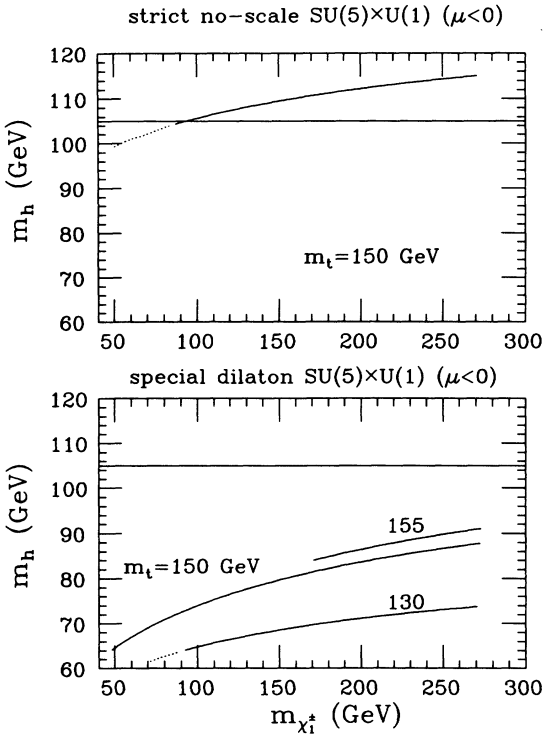

FIG. 16. The lightest one-loop corrected Higgs-boson mass vs tanβ in the strict no-scale (for $m_t = 150$ GeV) and the special dilaton (for $m_t = 130, 150, 155$ GeV) SU(5)×U(1) supergravity scenarios. The horizontal line marks the limit of sensitivity of LEP II with $\sqrt{s} = 200$ GeV. Note that LEP II should be able to explore all of the parameter space in the special dilaton scenario.

In Fig. 17 there are some points which "fall off" the main curve. These correspond to suppressed values of the $h \to b\bar{b}$ branching fraction (i.e., $f < 1$) which occur when the invisible supersymmetric decay channel $h \to \chi_1^0 \chi_1^0$ is kinematically open [64], as shown in Fig. 18. However, the fraction of points in parameter space where this happens is rather small (less than 10%). Nonetheless, most of these special points are still within the limit of sensitivity in Eq. (21) and should not escape detection. The scarcity of points in parameter space where the Higgs boson could decay invisibly may discourage detailed studies of such signature in SU(5)×U(1) supergravity. However, when the invisible mode is allowed, its branching fraction can be as large as 60%.

We can see the effect on the parameter space of a possible measurement of m_h by studying the Higgs-boson mass contours shown in Fig. 14, or for the full parameter space in Fig. 19. In general one would obtain a constraint giving tanβ for a given chargino mass. Moreover, a minimum value of the chargino mass would be required, if $m_h \gtrsim 100$ GeV. Furthermore, in the strict no-scale and special dilaton scenarios, the chargino mass itself would be determined (see Fig. 16) and thus the whole spectrum. If only a lower bound on m_h is obtained, still large portions of the parameter space could be excluded, i.e., all of the areas to the left of the corresponding mass contour.

What if $m_t > 150$ GeV? For $m_t = 170$ GeV, one obtains $m_h \lesssim 128$ GeV and $\sqrt{s} = 240$ GeV would be required for a full exploration of the parameter space at LEP II.

We close this section with a last-minute remark. Two-loop QCD corrections to m_h have been recently shown to decrease the Higgs-boson mass by a non-negligible amount [65]. A complete calculation of this effect in SU(5)×U(1) supergravity is beyond the scope of this paper. A rough assessment of the effects indicates that the Higgs-boson mass contours in Fig. 19 (see also Fig. 14) would likely shift to lower values. This downward shift implies an enlarged reach for LEP II. Equivalently, the above conclusions would require even lower values of the center-of-mass energy or integrated luminosity.

2. *Charginos*

The cross section for chargino pair production is the largest of all cross sections involving charginos and neu-

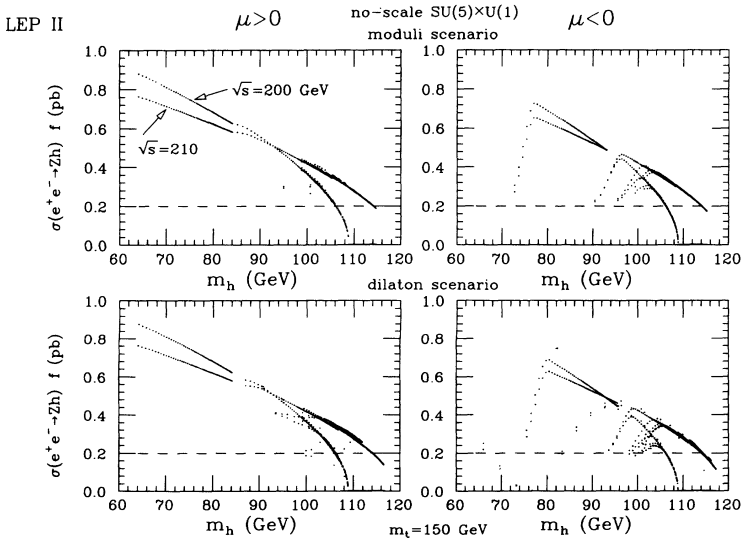

FIG. 17. The cross section $\sigma(e^+e^- \to Zh) \times f$ vs m_h at LEP II for $\sqrt{s} = 200, 210$ GeV and $m_t = 150$ GeV in the moduli and dilaton SU(5)×U(1) supergravity scenarios. Here $f = B(h \to b\bar{b})/B(H_{SM} \to b\bar{b})$. Except for the relatively few points deviating from the main curves, the result is very close to the standard model one. The dashed line indicates the expected level of sensitivity attainable at LEP II.

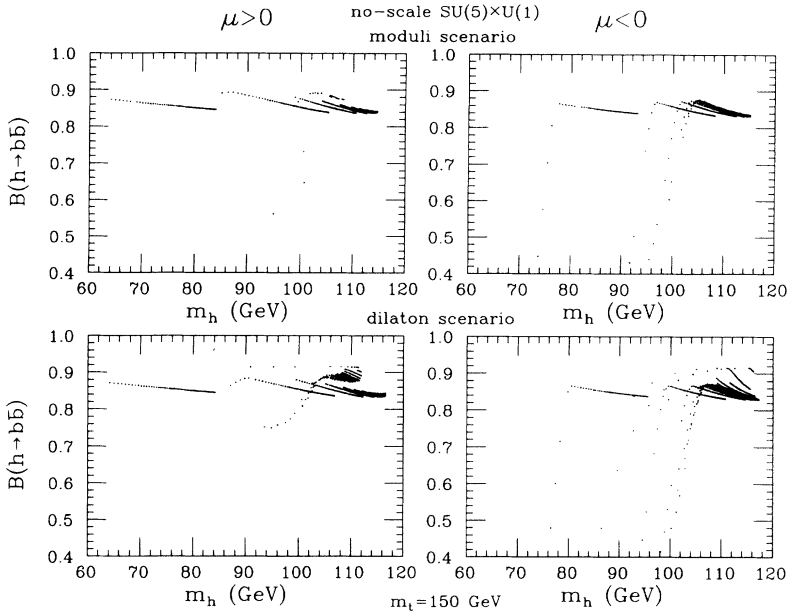

FIG. 18. The branching fraction $B(h \to b\bar{b})$ vs m_h for $m_t = 150$ GeV in the moduli and dilaton SU(5)×U(1) supergravity scenarios. Note the points which deviate significantly from the standard model expectation (of ≈ 0.85) owing to the contribution to the total width from the $h \to \chi_1^0 \chi_1^0$ channel.

tralinos at LEP II. In the context of SU(5)×U(1) supergravity this has been shown in Ref. [64]. The most studied signature is the so-called mixed mode, where one chargino decays leptonically and the other one hadronically. If the chargino decay channels are dominated by W exchange (i.e., branching ratio into electron+muon is $\frac{2}{9}$ and branching ratio into jets is $\frac{2}{3}$) then the mixed channel has a rate six times larger than the dilepton channel. The mixed signature still has to contend with the W^+W^- background. However, a series of cuts have been designed which take advantage of different values for the missing mass, the mass of the hadronic system,

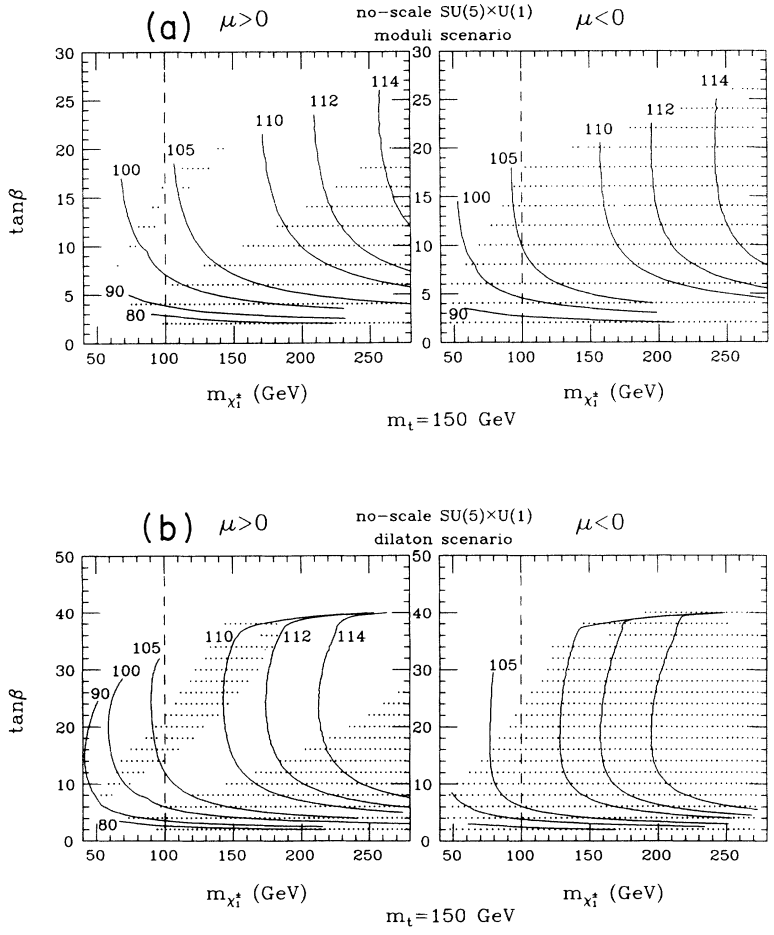

FIG. 19. The Higgs-boson mass contours in the $(m_{\chi_1^\pm}, \tan\beta)$ plane for $m_t = 150$ GeV in the (a) moduli and (b) dilaton SU(5)×U(1) supergravity scenarios. The dots represent the still-allowed points in parameter space. For $\mu < 0$ in the dilaton case, the labeling of the mass contours is as for $\mu > 0$.

and the mass of the lepton+neutrino system when one considers the background and the signal separately [66]. In the case of SU(5)×U(1) supergravity, W exchange is not expected to dominate in chargino decay [25]. In fact, in the moduli scenario the sleptons are lighter and can therefore be on shell, thus enhancing the leptonic branching fraction to its maximum value of $\frac{2}{3}$. When this occurs the mixed signal is negligible, because of the much suppressed hadronic branching fraction. In Fig. 20 we show the cross section for the mixed signal at LEP II for $\sqrt{s}=200$ GeV and $m_t=150$ GeV, for both moduli and dilaton scenarios. As expected, the mixed rate is small (even vanishing for $\mu<0$!) in the moduli scenario. In the dilaton scenario the rate is larger, but still much smaller than the corresponding rate in a model where W exchange dominates chargino decays. This situation in fact occurs in the minimal SU(5) supergravity model where the rate is typically in the range of (1.5–2) pb, as shown in Fig. 3 of Ref. [25]. The signal is further suppressed in the dilaton scenario because of a negative interference effect between the t-channel sneutrino-exchange and the s-channel γ^* and Z^* exchange [64]. Despite all these suppression factors, the mixed signal is still quite observable, as we now discuss.

The various cuts on the W^+W^- background mentioned above manage to suppress it down to 9 fb [66], while the signal (assuming W-exchange dominance) is suppressed by a factor of about $\epsilon=0.4$. Assuming that ϵ is not too different in our case, to observe a 5σ effect one would require

$$\frac{\epsilon(\sigma B)_{\text{mixed}}\mathcal{L}}{\sqrt{0.009\mathcal{L}}}>5 \Longrightarrow (\sigma B)_{\text{mixed}}>\frac{1.18}{\sqrt{\mathcal{L}}}=\begin{cases}0.12\text{ pb}, & \mathcal{L}=100\text{ pb}^{-1},\\ 0.05\text{ pb}, & \mathcal{L}=500\text{ pb}^{-1}.\end{cases} \tag{22}$$

The sensitivity limit obtained in this way for $\mathcal{L}=500$ pb^{-1} is shown as a horizontal dashed line on Fig. 20. The points in parameter space which would be probed in this way are marked by crosses (×) in Fig. 14. In the dilaton scenario one could thus probe nearly all points up to the kinematical limit (i.e., $m_{\chi_1^\pm}<100$ GeV).

Before concluding this section, let us examine the dilepton mode in chargino pair production, since in the moduli scenario it is likely to have a much larger rate than the mixed mode does. The dilepton rate is shown in Fig. 21 for both scenarios. The real problem here is the taming of the irreducible dilepton background from W^+W^- production, i.e., $\sigma(e^+e^-\to W^+W^-\to l^+\nu_l l^-\bar{\nu}_l)\approx(18)(\frac{2}{9})(\frac{2}{9})=0.9$ pb at $\sqrt{s}=200$ GeV. Cuts are apparently not very efficient in suppressing this background [67], although a reassessment of this problem needs to be performed to be certain. In any event, demanding that the dilepton signal have a 5σ significance over this background implies

$$\frac{(\sigma B)_{\text{dilepton}}\mathcal{L}}{\sqrt{0.9\mathcal{L}}}>5 \Longrightarrow (\sigma B)_{\text{dilepton}}>\begin{cases}0.47\text{ pb}, & \mathcal{L}=100\text{ pb}^{-1},\\ 0.21\text{ pb}, & \mathcal{L}=500\text{ pb}^{-1}.\end{cases} \tag{23}$$

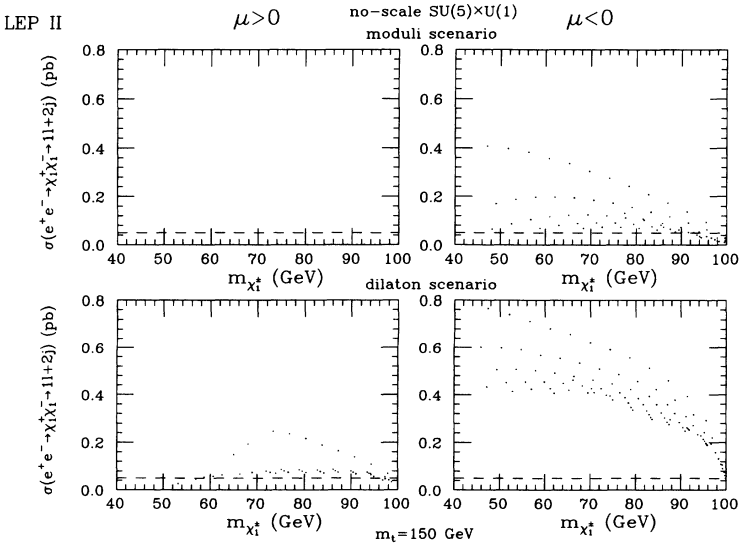

FIG. 20. The cross section $\sigma(e^+e^-\to\chi_1^+\chi_1^-\to 1l+2j)$ vs $m_{\chi_1^\pm}$ for chargino searches through the mixed mode at LEP II ($\sqrt{s}=200$ GeV) for $m_t=150$ GeV in the moduli and dilaton SU(5)×U(1) supergravity scenarios. The dashed lines indicate an estimated limit of sensitivity with $\mathcal{L}=500$ pb^{-1}.

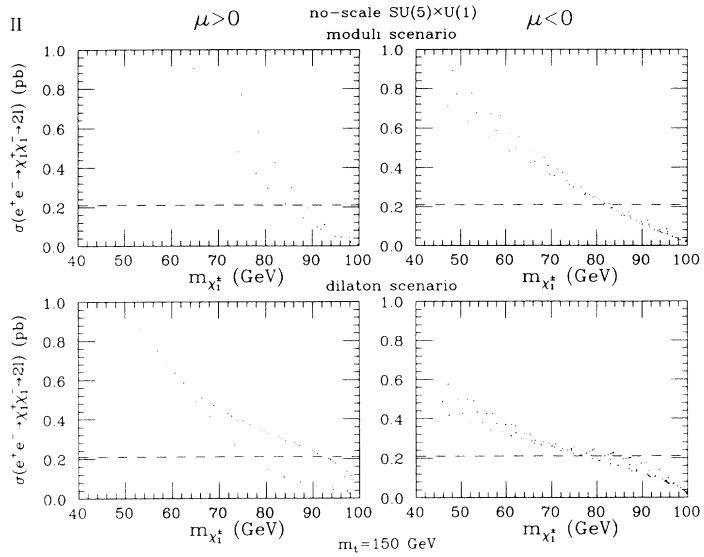

FIG. 21. The cross section $\sigma(e^+e^-\to\chi_1^+\chi_1^-\to 2l)$ vs $m_{\chi_1^\pm}$ for chargino searches through the dilepton mode at LEP II ($\sqrt{s}=200$ GeV) for $m_t=150$ GeV in the moduli and dilaton SU(5)×U(1) supergravity scenarios. The dashed lines indicate an estimated limit of sensitivity with $\mathcal{L}=500$ pb^{-1}.

This sensitivity limit is shown as a dashed line in Fig. 21. The regions of parameter space possibly explorable in this way are not shown in Fig. 14 since the dielectron signal from selectron pair production (discussed next) is much larger. Moreover, only 25% of the dilepton signal from chargino pair production consists of dielectrons.

3. *Sleptons*

The charged sleptons ($\tilde{e}_{L,R},\tilde{\mu}_{L,R},\tilde{\tau}_{L,R}$) could be pair produced at LEP II if light enough, and offer an interesting supersymmetric signal through the dilepton decay mode. In the moduli scenario there is a significant portion of the parameter space where these particles are kinematically accessible at LEP II, while in the dilaton scenario the accessible region is very small and will be neglected in what follows. The cross sections of interest are

$$e^+e^-\to\tilde{e}_L^+\tilde{e}_L^-,\tilde{e}_R^+\tilde{e}_R^-,\tilde{e}_L^\pm\tilde{e}_R^\mp\ , \tag{24}$$

$$e^+e^-\to\tilde{\mu}_L^+\tilde{\mu}_L^-,\tilde{\mu}_R^+\tilde{\mu}_R^-\ , \tag{25}$$

$$e^+e^-\to\tilde{\tau}_L^+\tilde{\tau}_L^-,\tilde{\tau}_R^+\tilde{\tau}_R^-\ . \tag{26}$$

The $\tilde{e}_L^+\tilde{e}_L^-,\tilde{e}_R^+\tilde{e}_R^-$ final states receive contributions from s-channel γ^* and Z^* exchanges and t-channel χ_i^0 exchanges, while the $\tilde{e}_L^\pm\tilde{e}_R^\mp$ only proceeds through the t-channel. The $\tilde{\mu}_L^+\tilde{\mu}_L^-$, $\tilde{\mu}_R^+\tilde{\mu}_R^-$, and $\tilde{\tau}_L^+\tilde{\tau}_L^-,\tilde{\tau}_R^+\tilde{\tau}_R^-$ final states receive only s-channel contributions, since all couplings are lepton flavor conserving, and therefore mixed LR final states are not allowed for smuon or stau production. In Fig. 22 we show the total selectron and total smuon cross sections, which include all the kinematically accessible final states mentioned above. The results for stau pair production are very similar to those for smuon pair production. The horizontal line represents an estimate of the limit of sensitivity achievable with $\mathcal{L}=500$ pb^{-1}, as given in Eq. (23) to observe a 5σ signal over the irreducible W^+W^- dilepton background. The selectron cross section is considerably larger than the smuon one because of the additional production channels.

Our discussion in effect assumes that the acoplanar

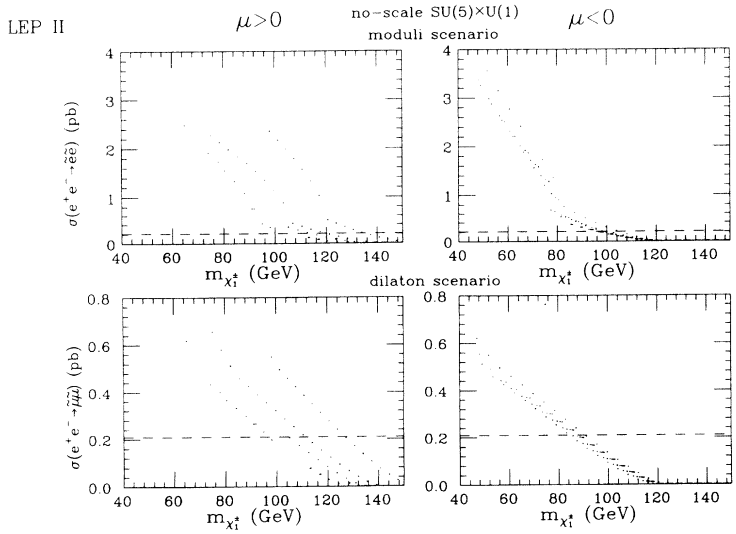

FIG. 22. The cross sections $\sigma(e^+e^-\to\tilde{e}\tilde{e})$ and $\sigma(e^+e^-\to\tilde{\mu}\tilde{\mu})$ vs $m_{\chi_1^\pm}$ for selectron and smuon searches at LEP II ($\sqrt{s}=200$ GeV) for $m_t=150$ GeV in the moduli and dilaton SU(5)×U(1) supergravity scenarios. The dashed lines indicate an estimated limit of sensitivity with $\mathcal{L}=500$ pb^{-1}. Note that slepton searches extend the indirect reach of LEP II for chargino masses, beyond $m_{\chi_1^\pm}\approx 100$ GeV.

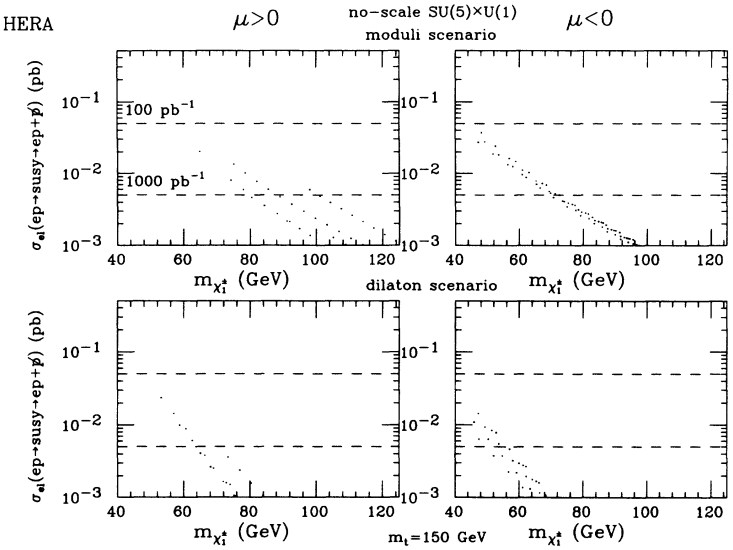

FIG. 23. The total elastic supersymmetric cross section (including selectron-neutralino and sneutrino-chargino production) at HERA vs $m_{\chi_1^\pm}$ for $m_t=150$ GeV in the moduli and dilaton SU(5)×U(1) supergravity scenarios. The dashed lines indicate limits of sensitivity with $\mathcal{L}=100$ and 1000 pb^{-1}.

dilepton signal associated with selectron pair production comes entirely from $\tilde{e}_{L,R}^{\pm}\to e^{\pm}\chi_1^0$ decay channels, i.e., purely dielectrons, and similarly for the smuon case. This is an approximation which holds fairly well in the moduli scenario [64].

The points in parameter space in the moduli scenario which would be explorable through selectron searches at LEP II are shown in Fig. 14 as diamonds (◇). The corresponding points explorable through smuon searches are not shown since the signal is smaller than in the selectron case. A rather interesting result is that the indirect reach in the chargino mass can be extended beyond the direct reach (of about 100 GeV). This effect depends on the value of tanβ, and is relevant only for tan$\beta\lesssim 6$ and $\mu>0$, as Fig. 14 shows. In fact, the three dotted lines for $\mu>0$ in Fig. 22 correspond from left to right to tan$\beta=6,4,2$ respectively.

C. HERA

The weakly interacting sparticles may be detectable at HERA in SU(5)×U(1) supergravity [68]. However, the mass range accessible is rather limited, with only the moduli scenario being partially reachable. The elastic scattering signal, i.e., when the proton remains intact, is the most promising one. The deep-inelastic signal has smaller rates and is plagued with large backgrounds [68]. The reactions of interest are $e^-p\to\tilde{e}_{L,R}^-\chi_{1,2}^0 p$ and $e^-p\to\tilde{\nu}_e\chi_1^- p$. The total elastic supersymmetric signal is shown in Fig. 23 versus the chargino mass. The dashed lines represent limits of sensitivity with $\mathcal{L}=100$ and 1000 pb^{-1} which will yield five "supersymmetric" events. This is a rather small signal. Moreover, considering the timetable for the LEP II and HERA programs, it is quite likely that LEP II would explore all of the HERA accessible parameter space before HERA does. This outlook may change if new developments in the HERA program would give priority to the search for the right-handed selectron ($\tilde{e}_R$) which could be rather light in the moduli scenario of SU(5)×U(1) supergravity.

VI. PROSPECTS FOR INDIRECT EXPERIMENTAL DETECTION

In Sec. III we discussed four indirect [i.e., $B(b\to s\gamma)$, $(g-2)_\mu$, neutrino telescopes, and $\epsilon_1-\epsilon_b$] and two direct (i.e., trileptons and the lightest Higgs-boson mass at LEP I) experimental constraints on the parameter space of SU(5)×U(1) supergravity. Of the indirect constraints, the neutrino telescopes probe may become strict in the not-so-distant future [i.e., when the Monopole, Astrophysics, and Cosmic Ray Observatory (MACRO) comes into operation], however the implicit assumption of significant neutralino population in the galactic halo cannot be verified directly, and this diminishes the weight to be assigned to this constraint. The $\epsilon_1-\epsilon_b$ constraint on the top-quark mass should become stricter with the reduction of the present error bars by a factor of 2 by the end of the LEP I program. In this section we examine the two remaining indirect constraints [$B(b\to s\gamma)$ and $(g-2)_\mu$] for the still-allowed points in parameter space.

In Fig. 24 we show the values of $B(b\to s\gamma)$ calculated for the still-allowed points in parameter space (for $m_t=150$ GeV) in the moduli and dilaton scenarios. For reference, the whole range of possible values before the imposition of the constraints discussed in Sec. III is addressed in Refs. [19,20]. In the moduli case, for $\mu>0$ one obtains a set of orderly lines for the indicated values of tanβ, which keep increasing in steps of two beyond the values explicitly noted. In the dilaton scenario the qualitative picture is somewhat similar, but for $\mu<0$ there is a somewhat wider range of possible values. For comparison, in the standard model for $m_t=150$ GeV one gets $B(b\to s\gamma)_{\rm SM}\approx 4\times 10^{-4}$ (although QCD corrections need to be accounted for carefully). A more precise measurement of this branching fraction should be used to exclude points in parameter space which deviate significantly from the standard model prediction. A detailed calculation of the QCD corrections in the supersymmetric case

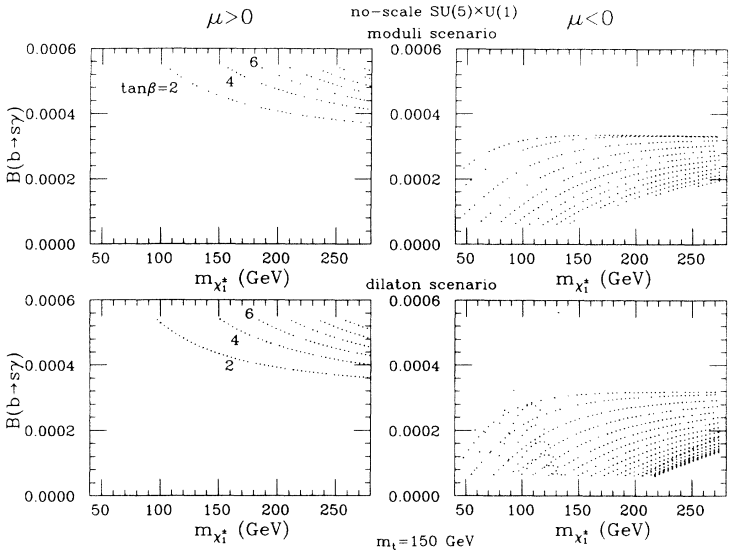

FIG. 24. The value of $B(b\rightarrow s\gamma)$ vs the chargino mass for the still-allowed points in parameter space with $m_t=150$ GeV in the moduli and dilaton SU(5)×U(1) supergravity scenarios. Wherever possible some values of tanβ have been indicated.

would be required to make a careful comparison with the standard model predictions.

In Fig. 25 we show the values of $a_\mu^{\rm SUSY}$ versus the gluino mass for $m_t=150$ GeV in the moduli and dilaton scenarios. Reference values of tanβ are indicated. The dotted portions of the lines correspond to points in parameter space excluded by the combined constraints in Sec. III. Note that for $\mu>0$ in both scenarios there is a range of $a_\mu^{\rm SUSY}$ values which is excluded for all values of tanβ. The new Brookhaven E821 experiment is expected to achieve a precision of 0.4×10^{-9}, which would entail a determination of tanβ as a function of the gluino (or chargino) mass. We remark that the supersymmetric contributions to a_μ could be so large that the uncertainty in the standard model prediction (1.76×10^{-9}) would be basically irrelevant when testing a large fraction of the allowed parameter space.

VII. CONCLUSIONS

We have presented an analysis of the several direct and indirect experimental constraints which exist at present on the parameter space of SU(5)×U(1) supergravity in the moduli and dilaton scenarios and their special cases (strict no scale and special dilaton). These scenarios are inspired by possible model-independent supersymmetry breaking scenarios in string models, and have the nonautomatic virtue of implying universal soft-supersymmetry-breaking parameters. The scenarios can be described in terms of three parameters ($m_{\chi_1^\pm}$, tanβ, m_t) which will be reduced down to two once the top-quark mass is measured. This minimality of parameters is very useful in correlating the many experimental predictions and constraints on the model. The ($m_{\chi_1^\pm}$, tanβ) plane (for

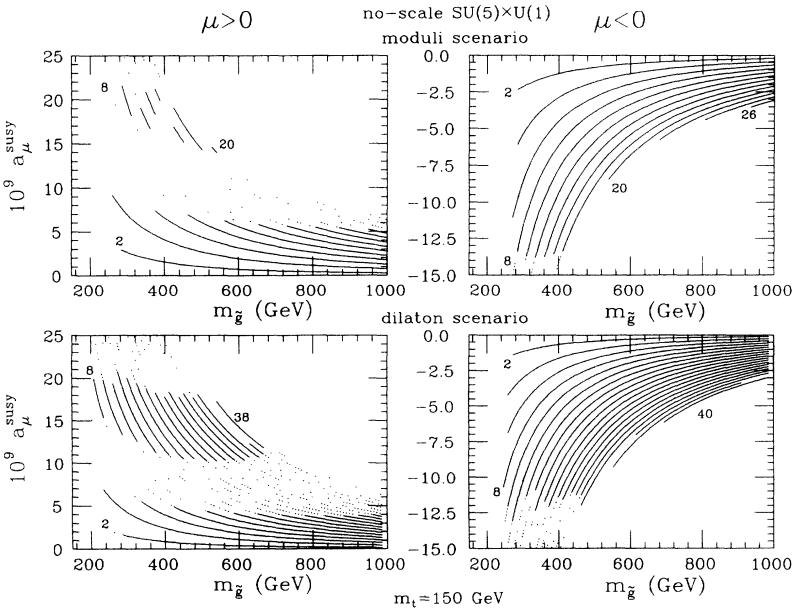

FIG. 25. The value of $a_\mu^{\rm SUSY}$ vs the gluino mass for $m_t=150$ GeV in the moduli and dilaton SU(5)×U(1) supergravity scenarios. The dotted portions of the curves are excluded. Some values of tanβ have been indicated.

fixed m_t) has been discretized and each point scrutinized to determine if the theoretical and basic LEP experimental constraints are satisfied. For satisfactory points we have then computed $B(b\to s\gamma)$, $(g-2)_\mu$, the rate of underground muon fluxes, $\epsilon_1-\epsilon_b$, and the trilepton rate at the Tevatron. Generally we find $m_t \lesssim 180$ GeV to satisfy the $\epsilon_1-\epsilon_b$ constraint, and some excluded regions of parameter space for specific values of m_t.

For the still-allowed points in parameter space we have reevaluated the experimental situation at the Tevatron, LEP II, and HERA. We have delineated the region of parameter space that would be explored in the 1994 Tevatron run, and by Higgs-boson, slepton, and chargino searches at LEP II with $\mathcal{L}=500$ pb^{-1}. With estimates for the possible sensitivities at these colliders, we conclude that the Tevatron could explore the parameter space with chargino masses as high as 100 GeV. On the other hand, searches for the lightest Higgs boson at LEP II could explore all of the allowed parameter space in both scenarios if $m_t \lesssim 150$ GeV and the beam energy is raised up to $\sqrt{s}=210$ GeV (or lower if the two-loop QCD corrections to m_h are accounted for). In fact, a measurement of the Higgs-boson mass in the standard model will almost uniquely determine the mass of the lightest Higgs boson in SU(5)×U(1) supergravity, since the relevant cross section and branching fractions deviate little from their standard model counterparts. Because of the mass correlations in the model, searches for selectrons allow LEP II to reach into the parameter space beyond the direct reach for chargino masses (i.e., $m_{\chi_1^\pm}<100$ GeV), thus selectrons are the next-deepest probe of the parameter space (after the Higgs boson), and charginos are the third probe. Searches for sparticles at HERA are not competitive with those at LEP II, although supersymmetric particles in the moduli scenario (in particular the right-handed selectron $\tilde{e}_R$) may be light enough to be eventually observed at HERA. Searches for strongly interacting sparticles (squarks and gluinos) are not kinematically favored at the Tevatron since, for example, chargino masses of 100 GeV correspond to gluino and squark masses around 400 GeV. All of these possible constraints from future direct particle searches have been shown in plots of the still-allowed points in parameter space (see Fig. 14). These plots show the regions where the various searches are sensitive and should serve as a "clearing house" where the many experimental constraints are brought in, enforced, and their implications discussed.

Let us conclude with a few general remarks in the context of SU(5)×U(1) supergravity (see Fig. 14).

If the Tevatron sees sparticles (charginos), then almost certainly would LEP II see sparticles, too.

If the Tevatron does not see sparticles (charginos), not much can be said about the prospects at LEP II.

It is quite possible that LEP II would see the lightest Higgs boson but no sparticles, if the Higgs-boson mass exceeds some m_t-dependent limit ($m_h \gtrsim 105$ GeV for $m_t=150$ GeV).

It is unlikely, although possible that LEP II would see sparticles but no Higgs boson.

If LEP II sees the lightest Higgs boson, then we would get a line in the $(m_{\chi_1^\pm},\tan\beta)$ plane, i.e., $\tan\beta$ as a function of $m_{\chi_1^\pm}$ (for fixed or known m_t). The measurement would be conclusive by itself only in the strict moduli and special dilaton scenarios.

If the Higgs boson, and selectrons or charginos are seen at LEP II, this should be enough to test the model decisively because of the predicted correlations among the various predictions.

In summary, the analytical procedure proposed in this paper could be applied to any supergravity model, and would serve as a standard against which the feasibility of various models could be measured and compared.

Note added in proof. An improved calculation of $B(b\to s\gamma)$ has been recently found to exclude some more points than those marked by pluses in Figs. 6–8. The subsequent calculations in the paper remain unaffected by this change. We also note that the values of the ("running") top-quark mass considered here $m_t=130$, 150, 170, 180 GeV correspond to somewhat higher values of the "pole mass," i.e., $m_t^{\rm pole}=139$, 160, 181, 192 GeV. Finally, the recent announcement by the CDF Collaboration of evidence for the top quark ($m_t^{\rm pole}=174\pm17$ GeV) appears to disfavor the $\mu>0$ possibility in the strict no-scale scenario (Sec. II D 1), which requires $m_t \lesssim 135$ GeV $\Longleftrightarrow m_t^{\rm pole}\lesssim 144$ GeV.

ACKNOWLEDGMENTS

We would like to thank James White and Teruki Kamon for useful discussions. This work has been supported in part by U.S. DOE Grant No. DE-FG05-91-ER-40633. The work of G.P. and X.W. has been supported by the World Laboratory.

[1] For a recent review, see J. L. Lopez, D. V. Nanopoulos, and A. Zichichi, in *From Superstrings to Supergravity,* Proceedings of the INFN Eloisatron Project 26th Workshop, edited by M. J. Duff, S. Ferrara, and R. R. Khuri (World Scientific, Singapore, 1993).

[2] I. Antoniadis, J. Ellis, J. Hagelin, and D. V. Nanopoulos, Phys. Lett. B **194**, 231 (1987).

[3] See, e.g., J. Ellis, J. L. Lopez, and D. V. Nanopoulos, Phys. Lett. B **245**, 375 (1990); A. Font, L. Ibáñez, and F. Quevedo, Nucl. Phys. **B345**, 389 (1990).

[4] I. Antoniadis, J. Ellis, J. Hagelin, and D. V. Nanopoulos, Phys. Lett. B **231**, 65 (1989).

[5] J. L. Lopez and D. V. Nanopoulos, Phys. Lett. B **251**, 73 (1990).

[6] J. L. Lopez, D. V. Nanopoulos, and K. Yuan, Nucl. Phys. **B399**, 654 (1993).

[7] I. Antoniadis, J. Ellis, R. Lacaze, and D. V. Nanopoulos, Phys. Lett. B **268**, 188 (1991).

[8] S. Kalara, J. L. Lopez, and D. V. Nanopoulos, Phys. Lett. B **269**, 84 (1991).
[9] S. Kelley, J. L. Lopez, and D. V. Nanopoulos, Phys. Lett. B **278**, 140 (1992); G. Leontaris, *ibid.* **281**, 54 (1992).
[10] J. L. Lopez, D. V. Nanopoulos, and A. Zichichi, Phys. Rev. D **49**, 343 (1994).
[11] L. Ibáñez and D. Lüst, Nucl. Phys. **B382**, 305 (1992).
[12] V. Kaplunovsky and J. Louis, Phys. Lett. B **306**, 269 (1993).
[13] A. Brignole, L. Ibáñez, and C. Muñoz, Report No. FTUAM-26/93, 1993 (unpublished).
[14] J. Ellis and D. V. Nanopoulos, Phys. Lett. **110B**, 44 (1982).
[15] J. Ellis, C. Kounnas, and D. V. Nanopoulos, Nucl. Phys. **B241**, 406 (1984); **B247**, 373 (1984); J. Ellis, A. Lahanas, D. V. Nanopoulos, and K. Tamvakis, Phys. Lett. **134B**, 429 (1984).
[16] For a review see A. B. Lahanas and D. V. Nanopoulos, Phys. Rep. **145**, 1 (1987).
[17] J. L. Lopez, D. V. Nanopoulos, and A. Zichichi, Phys. Lett. B **319**, 451 (1993).
[18] S. Kelley, J. L. Lopez, D. V. Nanopoulos, H. Pois, and K. Yuan, Nucl. Phys. **B398**, 3 (1993).
[19] J. L. Lopez, D. V. Nanopoulos, and G. T. Park, Phys. Rev. D **48**, R974 (1993).
[20] J. L. Lopez, D. V. Nanopoulos, G. T. Park, and A. Zichichi, Phys. Rev. D **49**, 355 (1994).
[21] J. L. Lopez, D. V. Nanopoulos, and X. Wang, Phys. Rev. D **49**, 366 (1994).
[22] J. L. Lopez, D. V. Nanopoulos, G. T. Park, H. Pois, and K. Yuan, Phys. Rev. D **48**, 3297 (1993).
[23] J. L. Lopez, D. V. Nanopoulos, G. T. Park, and A. Zichichi, Phys. Rev. D **49**, 4835 (1994).
[24] R. Gandhi, J. L. Lopez, D. V. Nanopoulos, K. Yuan, and A. Zichichi, Phys. Rev. D **49**, 3691 (1994).
[25] J. L. Lopez, D. V. Nanopoulos, X. Wang, and A. Zichichi, Phys. Rev. D **48**, 2062 (1993).
[26] J. Ellis and G. L. Fogli, Phys. Lett. B **249**, 543 (1990); J. Ellis, G. L. Fogli, and E. Lisi, *ibid.* **274**, 456 (1992); **292**, 427 (1992); **318**, 154 (1993); F. Halzen, B. Kniehl, and M. L. Stong, Z. Phys. C **58**, 119 (1993); F. del Aguila, M. Martinez, and M. Quiros, Nucl. Phys. **B381**, 451 (1992).
[27] U. Amaldi *et al.*, Phys. Rev. D **36**, 1385 (1987); G. Costa *et al.*, Nucl. Phys. **B297**, 244 (1988).
[28] J. Ellis, S. Kelley, and D. V. Nanopoulos, Phys. Lett. B **249**, 441 (1990); P. Langacker and M.-X. Luo, Phys. Rev. D **44**, 817 (1991); U. Amaldi, W. de Boer, and H. Fürstenau, Phys. Lett. B **260**, 447 (1991); F. Anselmo, L. Cifarelli, A. Peterman, and A. Zichichi, Nuovo Cimento **104A**, 1817 (1991).
[29] G. Altarelli, in *Proceedings of the International Europhysics Conference on High Energy Physics,* Marseille, France, 1993, edited by J. Carr and M. Perrottet (Editions Frontières, Gif-sur-Yvette, 1993).
[30] J. Ellis, G. L. Fogli, and E. Lisi, Phys. Lett. B **324**, 173 (1994).
[31] L. Ibáñez and G. Ross, Phys. Lett. **110B**, 215 (1982); K. Inoue *et al.*, Prog. Theor. Phys. **68**, 927 (1982); L. Ibáñez, Nucl. Phys. **B218**, 514 (1983); Phys. Lett. **118B**, 73 (1982); H. P. Nilles, Nucl. Phys. **B217**, 366 (1983); J. Ellis, D. V. Nanopoulos, and K. Tamvakis, Phys. Lett. **121B**, 123 (1983); J. Ellis, J. Hagelin, D. V. Nanopoulos, and K. Tamvakis, *ibid.* **125B**, 275 (1983); L. Alvarez-Gaumé, J. Polchinski, and M. Wise, Nucl. Phys. **B221**, 495 (1983); L. Ibáñez and C. López, Phys. Lett. **126B**, 54 (1983); Nucl. Phys. **B233**, 545 (1984); C. Kounnas, A. Lahanas, D. V. Nanopoulos, and M. Quirós, Phys. Lett. **132B**, 95 (1983); Nucl. Phys. **B236**, 438 (1984).
[32] L. Durand and J. L. Lopez, Phys. Lett. B **217**, 463 (1989); Phys. Rev. D **40**, 207 (1989).
[33] P. Nath and R. Arnowitt, Phys. Lett. B **289**, 368 (1992).
[34] J. L. Lopez, D. V. Nanopoulos, H. Pois, X. Wang, and A. Zichichi, Phys. Lett. B **306**, 73 (1993).
[35] M. Drees and M. Nojiri, Phys. Rev. D **45**, 2482 (1992).
[36] J. L. Lopez, D. V. Nanopoulos, and K. Yuan, Nucl. Phys. **B370**, 445 (1992).
[37] S. Kelley, J. L. Lopez, D. V. Nanopoulos, H. Pois, and K. Yuan, Phys. Rev. D **47**, 2461 (1993).
[38] See, e.g., E. Kolb and M. Turner, *The Early Universe* (Addison-Wesley, Reading, MA, 1990).
[39] J. E. Kim and H. P. Niles, Phys. Lett. **138B**, 150 (1984); Phys. Lett. B **263**, 79 (1991); E. J. Chun, J. E. Kim, and H. P. Nilles, Nucl. Phys. **B370**, 105 (1992).
[40] J. Casas and C. Muñoz, Phys. Lett. B **306**, 288 (1993).
[41] G. Giudice and A. Masiero, Phys. Lett. B **206**, 480 (1988).
[42] D0 Collaboration, S. Abachi *et al.*, Phys. Rev. Lett. **72**, 2138 (1994).
[43] E. Thorndike, Bull. Am. Phys. Soc. **38**, 922 (1993); CLEO Collaboration, R. Ammar *et al.*, Phys. Rev. Lett. **71**, 674 (1993).
[44] R. Barbieri and G. Giudice, Phys. Lett. B **309**, 86 (1993).
[45] N. Oshimo, Nucl. Phys. **B404**, 20 (1993); Y. Okada, Phys. Lett. B **315**, 119 (1993); R. Garisto and J. N. Ng, *ibid.* **315**, 372 (1993); F. Borzumati, Report No. DESY 93-090, 1993 (unpublished); M. Diaz, Phys. Lett. B **322**, 207 (1994).
[46] W. H. Press and D. N. Spergel, Astrophys. J. **296**, 679 (1985).
[47] A. Gould, Astrophys. J. **321**, 560 (1987); **321**, 571 (1987); **328**, 919 (1988); **388**, 338 (1992).
[48] D. Kennedy and B. Lynn, Nucl. Phys. **B322**, 1 (1989); D. Kennedy, B. Lynn, C. Im, and R. Stuart, *ibid.* **B321**, 83 (1989).
[49] M. Peskin and T. Takeuchi, Phys. Rev. Lett. **65**, 964 (1990); W. Marciano and J. Rosner, *ibid.* **65**, 2963 (1990); D. Kennedy and P. Langacker, *ibid.* **65**, 2967 (1990).
[50] B. Holdom and J. Terning, Phys. Lett. B **247**, 88 (1990); M. Golden and L. Randall, Nucl. Phys. **B361**, 3 (1991); A. Dobado, D. Espriu, and M. Herrero, Phys. Lett. B **255**, 405 (1991).
[51] G. Altarelli and R. Barbieri, Phys. Lett. B **253**, 161 (1990).
[52] G. Altarelli, R. Barbieri, and S. Jadach, Nucl. Phys. **B369**, 3 (1992).
[53] G. Altarelli, R. Barbieri, and F. Caravaglios, Nucl. Phys. **B405**, 3 (1993).
[54] R. Barbieri, M. Frigeni, and F. Caravaglios, Phys. Lett. B **279**, 169 (1992).
[55] G. Altarelli, R. Barbieri, and F. Caravaglios, Phys. Lett. B **314**, 357 (1993).
[56] G. Altarelli, CERN Report No. CERN-TH.6867/93, 1993 (unpublished).
[57] J. Ellis, J. Hagelin, D. V. Nanopoulos, and M. Srednicki, Phys. Lett. **127B**, 233 (1983); P. Nath and R. Arnowitt, Mod. Phys. Lett. A **2**, 331 (1987); R. Barbieri, F. Caravaglios, M. Frigeni, and M. Mangano, Nucl. Phys. **B367**, 28 (1991); H. Baer and X. Tata, Phys. Rev. D **47**, 2739 (1993); H. Baer, C. Kao, and X. Tata, *ibid.* **48**, 5175 (1993).
[58] Talk given by J. T. White (D0 Collaboration) at the 9th Topical Workshop on Proton-Antiproton Collider Physics, Tsukuba, Japan, 1993 (unpublished).

[59] Talk given by Y. Kato (CDF Collaboration) at the 9th Topical Workshop on Proton-Antiproton Collider Physics, Tsukuba, Japan, 1993 (unpublished).
[60] T. Kamon (private communication).
[61] A. Sopczak, L3 note 1543, 1993 (unpublished).
[62] J. L. Lopez, D. V. Nanopoulos, and X. Wang, Phys. Lett. B **313**, 241 (1993).
[63] See, e.g., J. Gunion, H. Haber, G. Kane, and S. Dawson, *The Higgs Hunter's Guide* (Addison-Wesley, Redwood City, 1990).
[64] J. L. Lopez, D. V. Nanopoulos, H. Pois, X. Wang, and A. Zichichi, Phys. Rev. D **48**, 4062 (1993).
[65] R. Hempfling and A. Hoang, DESY Report No. 93-162, 1993 (unpublished).
[66] J.-F. Grivaz, in *Properties of SUSY Particles,* Proceedings of the 23rd INFN Eloisatron Project Workshop, Erice, Italy, 1992, edited by L. Cifarelli and V. A. Khoze (World Scientific, Singapore, 1993).
[67] C. Dionisi *et al.*, in *Proceedings of the ECFA Workshop on LEP 200,* Aachen, West Germany, 1986, edited by A. Böhm and W. Hoogland (CERN Report No. 8708, Geneva, Switzerland, 1987), p. 380.
[68] J. L. Lopez, D. V. Nanopoulos, X. Wang, and A. Zichichi, Phys. Rev. D **48**, 4029 (1993).